LANDSAT TEMPORAL DISCRIMINATION OF FOREST COVER TYPES OF THE CARMANAH VALLEY, BRITISH COLUMBIA

by

SAMMY KIBET YATICH

B.Sc., Moi University, 1992

A THESIS SUBMITTED IN PARTIAL FULFILMENT OF

THE REQUIREMENTS FOR THE DEGREE OF

MASTER OF SCIENCE

in

THE FACULTY OF GRADUATE STUDIES

(Department of Forest Resource Management)

We accept this thesis as conforming

to the required standard

THE UNIVERSITY OF BRITISH COLUMBIA

February 1997

In presenting this thesis in partial fulfilment of the requirements for an advanced degree at the University of British Columbia, I agree that the Library shall make it freely available for reference and study. I further agree that permission for extensive copying of this thesis for scholarly purposes may be granted by the head of my department or by his or her representatives. It is understood that copying or publication of this thesis for financial gain shall not be allowed without my written permission.

Department of Forest Resources Management

The University of British Columbia
Vancouver, Canada

Date March 14, 1997

Abstract

The classification of forest cover types in the Pacific Coastal Rainforest is a difficult task. The complexity and variability of species compositions and sites makes various cover types arduous to define and identify. This study utilised multitemporal TM satellite data and a combined classification approach to determine if it is possible to discriminate forest cover types of the Carmanah Valley. Landsat TM data from June and September were used to investigate whether seasonal variability can aid in the discrimination.

Due to the huge dataset involved, principal component analysis (PCA) was applied to reduce data dimensionality to a level that could be easily handled or processed with available image analysis software and enhance the meaning. Results from PCA were used in visual analysis and supervised classification. Classification accuracies for three temporal data sets, June-early summer, September-late summer and a multitemporal set, were compared. Finally, TM data were assessed for their potential to provide information regarding forest age and stocking classes.

Results indicated that the degree of correlation between any two bands was related to the amount of spectral contrast. The higher the correlation, the less the spectral contrast and the lower the correlation, the more the spectral contrast. A trend was observed between stand age and digital values. With an increase in stand age, digital values decreased in all TM bands considered. However, the main funding was that the specific forest cover types of the Carmanah Valley can be identified and that time of the year can significantly affect cove-type classification accuracy. Comparison of the classifications of forest cover type showed that the multitempoal approach was significantly better than the single-date classifications.

Table of Contents

List of Tables

List of Figures

List of Abbreviations

EASI	Engineering Analysis and Scientific Interface
CHNSEL	Channel Selection
CV	Coefficient of Variation
DN	Digital Number
FCM	Forest Cover Map
FIRMS	Forest Resource Management System
GCP	Ground Control Point
GIC	Geographic Information Centre
GIS	Geographic Information System
IFOV	Instantaneous Field of View
IHS	Intensity, Hue and Saturation
IR	Infra Red
K-CLUS	K-means Clustering
MLC	Maximum-Likelihood Classifier
MSS	Multispectral Scanner
NDVI	Normalized Difference Vegetation Index
NUM	Numeric
PACE	Picture Analysis, Correction and Enhancement
PCA	Principal Component Analysis
PC1,2...,n	Principal Component 1, 2, ..., n
R^2	Coefficient of Determination
RGB	Red, Green and Blue Monitor
SAS	Statistical Analysis System
SE_E	Standard Error of Estimate
SIGSEP	Signature Separability
TM	Thematic Mapper
UBC	University of British Columbia
UTM	Universal Transverse Mercator

Acknowledgements

I would like to express my sincere gratitude to my supervisor, Dr. P. A. Murtha, for suggesting the study and under whose direction this study was undertaken. His patience, kindness, academic contribution and financial assistance were an immense support during the course of the study.

I am also grateful to the members of my supervisory committee: Dr. P. Marshall and Mr. D. Nazarenko who gave valuable assistance and for their constructive criticism of the draft. I thank Radarsat International for supplying TM data. Mr. J. Maedel provided me with lab space and considerable technical assistance for which I am really grateful.

Finally I wish to acknowledge the Government of Kenya for supporting my studies at UBC. Funding was also provided by the Donald S. McPhee Fellowship Fund. The department of Forest Resources Management gave assistance in the form of teaching assistantships.

Chapter 1

Introduction

As the world's population grows, the available land base declines. Planning and management of land resources become more complex. A partial solution to this complexity is a timely and reliable mechanism for acquiring land-use and land-cover information. Remote sensing is one tool that does provide this kind of information. It is such recent technologies in addition to traditional sources that have significantly improved our ability to manage our resources.

Over the last decade remote sensing applications have been developed which can meet a variety of mapping information needs. The user can choose from several remote sensing systems. The criteria for selecting a remote sensing system include the accuracy of the information it provides, scale, and the information content implicit in the data. For example, the Thematic Mapper of the Landsat series produces an order of magnitude more data per scene than Landsat Multispectral Scanner. Once a sensor is selected there is need to address the question of the appropriate time for image acquisition. The best season to acquire Landsat data for instance is often generalised with respect to weather conditions, usually avoiding periods of cloud cover. However, imagery acquired on different dates, weather conditions notwithstanding, provide a different information content.

Remote sensing has been applied widely in forest management planning. Aerial photographs, for example, have been used for many years by foresters as a tool to help monitor and manage forest resources. Aerial photographs are currently an integral part of most forest inventory programs. The

launch of Landsat-1 in 1972 added an entirely new dimension to the capability to obtain information on Earth resources. There has been an interest since that time in the potential of satellite data and computer-aided analysis techniques to detect, identify, quantify, and map forest resources. Attractive features of these data include repetitive coverage of large areas at short intervals (and consistent image quality), a digital data format allowing for fast processing of large amounts of data, and the potential for data incorporation into geographic information systems (GIS).

Forest resources are continually changing. Some forest cover modifications are human-induced, such as harvesting, while others have natural causes, such as insects or disease damage. The rate of change may be abrupt (e.g., logging) or gradual (e.g., growth). The potential for using satellite data to detect and characterise these changes depends on the ability to quantify temporal effects using multitemporal data sets. However, the intent in change detection is to compare spatial representations of two land cover types or selected features in time by controlling all variances caused by differences in variables not of interest. The basic premise thus is that changes in land cover must result in radiance values and changes in radiance due to land cover must be larger than changes in radiance caused by other factors (Ingram *et al.*, 1981). The other factors include differences in atmospheric conditions, differences in sun angle, and differences in soil moisture (Jensen, 1983). The impacts of these factors may be reduced by selecting the appropriate data (e.g., Landsat data belonging to the same season of the year).

Several methods of assessing the information content of Landsat TM data have been devised. These include interpretative analysis of the data in multidimensional feature space, computer-based classification of a scene, with emphasis on accuracy and detail, and computation of statistical measures of separability between cover classes (Horler and Ahern, 1986). In addition to relying on these

statistically based approaches, the interpreter's ability to extract information depends, among other things, on the method of colour presentation of the imagery, experience, and a thorough knowledge of the area under investigation.

The classification of forest cover types in the Pacific Coastal Rainforest is a difficult task. The complexity and variability of species compositions and sites makes various cover types hard to define and identify. The general purpose of this study is to test for temporal discrimination of the forest cover types of the Carmanah Valley in Vancouver Island, British Columbia. By using Landsat Thematic Mapper data acquired in June, 1992 and September, 1992, this study investigates whether seasonal variability can help in mapping forest cover types. Forest inventory variables, namely forest species composition, age class and stocking class resident in a GIS database, serve as reference data. Questions to be answered include: (a) what new forestry information does each TM band contribute that is not contained in the others? (b) are there any differences between oldgrowth and maturing forests in terms of spectral characteristics? (c) does seasonal variability affect classification accuracy? (d) by how much does topography influence classification of forest cover types? and (e) what level of forest classification does TM data provide? An additional objective of the study is to identify and measure the extent of change in the multitemporal data set using image differencing, image ratioing and the normalised difference vegetation index.

This document is divided into five chapters. Chapter 2 provides a brief introduction to remote sensing, and a review of previous studies on the research topic. The methods used are outlined in chapter 3. Study results are presented and discussed in chapter 4. Chapter 5 briefly concludes the study. Ground control points and polynomial transformation used in geometric correction are given in Appendix I. Appendix II provides signature "seperability" reports of training statistics and results of

some of the image analyses are presented in Appendix III. Analysis of variance tables are presented in Appendix IV.

Chapter 2

Background For The Study

2.1 Remote Sensing Defined

Remote sensing is defined as the science and art of obtaining information about an object, area, or phenomenon through the analysis of data acquired by a device that is not in contact with the object, area or phenomenon under investigation (Lilesand and Kiefer, 1994). It basically involves using electromagnetic radiation sensors to record images of the environment which can be interpreted to yield useful information.

The development of remote sensing dates back to early 1860s when photographs were successfully taken from balloons held to the ground (Aronoff, 1989). By the early 1900s photographic technology had improved to the point that smaller cameras and faster lenses and films were available. The 1960s ushered in a new age for remote sensing. It was during this time that visual interpretation of black and white aerial photographs paralleled research into the use of data from the new aircraft and satellite borne sensors. With the development of earth-orbiting satellites, it became feasible to obtain high altitude images of the earth's surface. More important was the development of digital electronic imaging systems that could relay image data back to earth. These data could be processed to photographic images using computer-based techniques known as image processing (Aronoff, 1989). In summary, remote sensing, especially non-photographic remote sensing, grew rapidly after the successful launch in 1972 of the Earth Resources Technology satellite (ERTS-1) later renamed Landsat

1 (Curran, 1985). This satellite, which carried sensors capable of providing synoptic views of the Earth's surface every 18 days, proved to be the harbinger of many of the interpretation techniques and image analysis softwares that are in use today.

Remote sensing is utilised in a wide range of disciplines. It's usefulness has been realised in the environmental sciences of geography, geology, botany, zoology, civil engineering, forestry, meteorology, agriculture and oceanography. The advantage of remote sensing over traditional methods has been documented in all these fields.

The two basic processes involved in electromagnetic remote sensing of earth resources are data acquisition and data analysis. However, the fundamental steps used to analyse all remotely sensed data include: (a) definition of information needs, (b) collection of data using remote sensing and other techniques, (c) data analysis - image processing, (d) verification of analysis results, (e) reporting of results to those who will use the information, (f) taking action based on the information (Aronoff, 1989). Data analysis and verification of results are the main focus of this study.

2.2 TM Spectral Regions and Their Principal Applications

The Landsat Thematic Mapper is a highly advanced multispectral scanner incorporating a number of spectral, radiometric, and geometric design improvements relative to MSS (Lilesand and Kiefer, 1994). Spectral attributes include acquisition of data in seven bands in the visible, near-infrared, shortwave infrared and thermal infrared as shown in Table 1. The wavelength range and location of the TM bands have been chosen to improve the spectral differentiability of major earth surface features and

Table 1. Thematic Mapper Spectral Bands (Adopted from Lilesand and Kiefer, 1994).

Band	Wavelength (nm)	Nominal Spectral Location and Remote Sensing Importance	Spatial Resolution (m)
1	450 - 520	Blue Water body penetration	30
2	520 - 600	Green Chlorophyll reflectance	30
3	630 - 690	Red Chlorophyll absorption	30
4	760 - 900	Near-infared Leaf structure reflectance and biomass content	30
5	1550 - 1750	Shortwave infrared (SWIR-1) Vegetation moisture content and soil moisture	30
6	10400 - 12500	Thermal infared Heat emission	120
7	2080 - 2350	Shortwave infrared (SWIR-2) Rocktype discrimination	30

are particularly more finely tuned for vegetation discrimination. Radiometrically, the TM performs its onboard analog-to-digital signal conversion over a quantization range of 256 digital numbers (8 bits). This finer radiometric precision permits observation of smaller changes in radiometric magnitudes in a given band and provides greater sensitivity to changes in relationships between bands. Geometrically, TM data are collected using a 30 metre instantaneous field of view (IFOV) for all bands except for the thermal band which has a 120 metre IFOV. Additionally, several design changes have been incorporated within the TM to improve the geodetic positioning of the data (Lilesand and Kiefer, 1994). Landsat-5 TM is best suited for vegetation discrimination. In particular, the spectral bands take advantage of distinctive characteristics of the spectral response of vegetation. Bands 1 and 3 were chosen to coincide with chlorophyll-absorption bands and band 2 with the chlorophyll-reflection peak. Whereas spectral response in the visible bands is controlled primarily by plant pigments, the response in the near-infrared sensed by band 4 is controlled mainly by the physical structure of the mesophyll layer of leaves (Townshend, 1984). Band 5 in the middle-IR is on the shoulder between two water-absorption bands. Band 7 was chosen primarily for identification of hydrothermally altered minerals in association with mineral exploration, but should have some potential for soil discrimination (Lilesand and Kiefer, 1994). Band 6 is in the thermal part of the spectrum and hence includes emitted radiation almost entirely. It is potentially useful in a range of thermal mapping applications.

2.3 PCA TM Data Reduction and Enhancement

Dimensional satellite data reduction and enhancement have proven useful in various mapping and information extraction purposes (Schonwengerdt, 1983) and also in digital change detection and characterising seasonal changes in cover types (Townshend *et al.*, 1983). A challenge encountered with raw Landsat TM data is to reduce the dataset and to display as much information as possible in a

three-image set colour composting. Principal component analysis (PCA) is one tool used to address this problem. Being a mathematical transformation, PCA generates new variables, referred to as components or axes, which are both orthogonal to each other and linear combinations of the original variables.

Results of PCA on images poses two problems. One is that information that is not mapped to the selected components can be of significant interest, depending on the degree of correlation and spectral contrast that exist among the six Landsat TM bands (Williams, 1983). The other problem is that a colour composite made from three of the six components can be difficult to visually interpret (Williams, 1983). Chavez and Kwarteng (1989) demonstrated that "selective" PCA can be used to minimise both of these problems.

Singh and Harrison (1985) reported that a significant improvement in signal-to-noise ratio and image enhancement is realised by employing the correlation rather than the variance-covariance matrix in the principal component analysis and that standardized principal components are more accurate than non-standardized components. They attributed the latter to better alignment along land-cover changes in the multitemporal data structure. The statistics that they extracted from the entire study area were better and more reliable than those extracted from the subset area.

2.4 TM Imagery for Forestry Applications

A relevant and accurate forest cover-type classification system is essential for providing necessary information for effective management of forest resources. Research aimed at developing methods for reliably classifying forest cover and habitat types dates back many decades and continues to this day (Eyre, 1980). Three approaches to the classification of habitat types have been outlined:

biophysical, forest type, and forest type/forest soil classifications. The single factor important to all three approaches is the classification of forestland into specific cover types.

Developments within the remote sensing community have shown promise for classification of forest cover types throughout the world. These developments indicate that increases in the accuracy of forest classifications can be expected by combining supervised and unsupervised classification techniques (Chuvieco and Congalton, 1988). In the combined approach, a set of spectrally and 'informationally' unique training statistics can be generated. This results in improved classification accuracy due to the improved grouping of training statistics (Green and Teply, 1991).

Unfortunately, fewer researchers have presented results from the use of actual TM data in forestry applications. However, significant results have so far been realised by taking advantage of the excellent spectral, spatial, and radiometric quality of TM data. DeGloria (1984) reported that higher TM spatial resolution provides the ability to discriminate small agricultural fields and boundaries, forest stand boundary conditions, road and stream networks in rough terrain, and small clearings resulting from various forest management practices. In their application of TM data to forest surveys in California, Benson and DeGloria (1985) concluded that the best TM data can provide higher classification accuracies than MSS data. The additional spectral information of TM bands 5 and 7 appeared largely responsible for the improved performance. Specifically, these bands seemed to be particularly sensitive to forest vegetation density, especially in the early stages of clear-cut regeneration.

Spanner *et al.* (1984) found that TM simulator data were able to discriminate, with fair accuracy, among two conifer size classes, three shrub-classes in regenerating cutovers, and four conifer crown closure classes. Successful separation of red and jack pine in TM data by Hopkins *et al.* (1988) indicates again a potential distinction of species or species groups. They suggested that at least one

band of each of the non-thermal wavelength regions of the TM (visible, near-IR, and shortwave-IR) is desirable for forestry applications.

Horler and Ahern (1986) emphasized feature selection, that is the determination and selection of optimal bands or band transforms, for visual enhancements of imagery of boreal forests. Shadowing was at least as important as leaf moisture content in influencing the spectral reflectance of forests. They concluded that TM data contain more spectral information on forest classes than MSS imagery. A limitation is that they based their conclusions on image enhancement rather than on classification performance.

Using only four bands Latty and Hoffer (1981) achieved a high separability between a number of forest classes - pine, pine-hardwood, old age hardwood, second growth hardwood, water tupelo, sycamore, and clearcuts. This suggests that fewer bands can perform as well as all six bands.

Recent emphasis on landscape and regional analyses necessitates monitoring forest regeneration over large areas. Conditions within regenerating stands change quickly and, therefore, stand information condition must be updated periodically. Analysis of remotely sensed data from satellites has potential for assessing forest regeneration and wildlife habitat because it provides coverage over large geographic areas on a regular basis (Fiorella and Ripple, 1993). TM data may be suitable to monitor within-stand condition because of the improved spatial and spectral resolution.

In an analysis of TM simulator data for 123 field sites in Sequoia National Park, Peterson *et al.* (1986) indicated that canopy closure could be estimated well by a variety of bands or band ratios without reference to forest type. Estimation of basal area was less successful on average. Within forest types, canopy closure appeared to be the best predictor of spectral variation.

Wolter *et al.* (1995) suggested that changes in spectral reflectance caused by phenological differences among temperate forest tree species may allow for Anderson III forest cover type classification on a regional scale. Specifically, large seasonal variation in forest species spectral response in the visible portion of the electromagnetic spectrum and phenological differences in senescence among tree species present unique forest classification opportunities (Eder, 1989).

Forest classifications using single date Landsat TM data have been demonstrated to be moderately successful in separating forest cover types. Not so with multitemporal TM data, where much better classification has been realized. In fact, the multitemporal approach was found to be useful for broad-scale forest cover monitoring in areas where ancillary data were not available (Wolter et al., 1995).

In their discrimination of coniferous forest, deciduous forest, and agricultural land using a maximum-likelihood decision rule, Kalensky and Scherk (1975) found that three dates of imagery from June, September, and October provided the best results (84 % mixed overall classification accuracy) over all other single- or multiple-date classifications tested. They concluded that, although the October, June and September MSS scenes individually produced low overall classification accuracies (67 percent, 69 percent, and 81 percent, respectively), their collective use mitigated the effects of individual image noise. Using MSS data for a classification of the Crater Lake National Park region, Walsh (1980) found that September imagery provided more information than early summer MSS data due to the phenological condition of vegetation and the lower sun angle.

In different regional settings, spectral response in visible and near infrared wavelengths measured by satellite and aerial sensors has been shown to vary significantly with forest attributes such as species, crown or canopy density, height, volume, health, and age (Horler and Ahern, 1986). In

mountainous areas, image variance can be influenced by the topographic effect (Leprieur *et al.*, 1988). Atmospheric constituents, size of the viewed area, and the geometrical and optical properties of the surface cover, underlying soil, and background may also contribute additional variance.

2.5 Mapping the Successional Stage of Temperate Conifers

Distinguishing old-growth from maturing forests has been difficult because both successional stages tend to have large trees, and high basal and leaf areas (Spanner *et al.*,1990). Most forest parameters such as biomass, leaf area index, volume, and, in general, vegetation amount have asymptotic relationships to single band spectral data beginning at moderate to high levels of these stand parameters (Horler and Ahern, 1986). Differences in old-growth and maturing forests are determined by a combination of overstory and understory structural and compositional factors from ground-based surveys. Unfortunately, remote sensing data primarily measure only canopy overstory characteristics. Two of the most important distinguishing features observed at the canopy level are differences in the number and size of gaps in the forest canopy and the heterogeneity of tree sizes (Spies *et al.*, 1990). In general, old-growth canopy gaps tend to be horizontally larger, but less numerous than those in maturing stands (Spies *et al.*, 1990). They observed that both of these features create dark shadows in old-growth forest canopies which contrast sharply with sunlit tree crowns.

Identifying forest successional stages in dissected mountainous terrain is complicated due to the dark shadowing on steep north-facing slopes and high variability in illumination conditions. Eby (1987) used Landsat MSS near-infrared band 4 imagery to identify old-growth forest stands with 80 percent accuracy. Sun incidence angle was used to stratify the study area into normally illuminated and shaded areas for post-classification sorting. Studies by Leprieur *et al.* (1988) also indicate that both sun

angle and plant architecture or canopy structure can influence measured reflectance. These factors in conjunction with slope can determine whether vegetation response to incident sun light is best modelled by a Lambertian or non-Lambertian model (Leprieur *et al.*, 1988). Unfortunately, previous work in the analysis of Thematic Mapper data related to forest canopy is limited, especially in mountainous areas.

2.6 Classification Accuracy

Thematic (categorical) maps are increasingly being used by people involved in management of natural resources. There is a need to assess the accuracy of these maps. Traditionally, the accuracy of a thematic map was determined by comparing the map with corresponding reference data or ground data. The results were tabulated in a square matrix whose columns usually represented the ground data (i.e., assumed correct) and the rows indicate the mapped or classified data. Each element in the matrix gave the number of areas assigned to a particular category relative to the ground data. Generally, the elements of the principal (diagonal) of the matrix represented correct matches, whereas the remaining cells were mismatches. This matrix is popularly known as an error or confusion matrix (Card, 1982) and forms the basis for a series of discrete analysis (Congalton, 1991).

Descriptive and analytical techniques are appropriate because remotely sensed data are discrete rather than continuous (Congalton, 1991). The data are binomially or multinormally distributed rather than normally distributed. Therefore, many common normal theory statistical techniques do not apply. Classification accuracy reviewed by Congalton (1991) listed ground data collection, classification scheme, spatial autocorrelation, sample size, and sampling scheme as important factors to consider when performing accuracy assessment. He cautioned that each of these factors provide essential

information for the assessment, and failure to consider even one of them could lead to serious shortcomings in the assessment process.

Acceleration of the acceptance of remotely sensed data requires addressing issues for which the remote sensing technologist is often not prepared. Included, for example, are such issues as cost/benefit in relation to traditional approaches, and accuracy of results. It has been demonstrated that the cost of data acquisition and analysis are markedly lower with satellite data than with ground surveys. Given the cost advantage, the discussion then becomes one of whether accuracy is sufficient when remotely sensed data are the principal source. Unfortunately, accuracy of land-use interpretation is a complex issue, in both definition and measurement. For example, an area delineated as a particular category may be in error for one or more of three reasons: classification error, boundary line error or control point location error (Hord and Brooner, 1976).

2.7 Change Detection

Remote sensing provides a viable source of data from which updated land-cover information can be extracted efficiently and cheaply. Thus, change detection has become a major application of remote sensing data (Fung and LeDrew, 1988). Visual comparison of air photos as a traditional change detection tool has been characterised as slow, tiring, and subject to errors of omission (Shepherd, 1964). He observed that there is need for a detector which can automatically correlate and compare two sets of imagery taken of the same area at different times and display the changes and their locations to the interpreter. With the availability of remote sensing imagery recorded in digital format and on repetitive coverage at short intervals, there have been substantial developments in digital change detection techniques. These techniques include image differencing, image ratioing, principal component

analysis, post-classification comparison, and multitemporal classification (Jensen, 1986).

Change detection techniques involve a transformation of the original spectral bands so as to enhance the land-cover changes. In image differencing, the same spectral bands at different dates are subtracted from each other pixel by pixel. Image ratioing uses division rather than subtraction to generate new images. Work by Vogelmann and Rock (1989) demonstrated that temporal image differencing techniques are powerful tools for characterising changes in forest canopy characteristics. Miller *et al.*, (1991) applied Landsat image differencing successfully in mapping changes in tropical forest cover in northern Thailand. Vegetation indices such as the normalised difference vegetation index (NDVI) derived from remotely sensed data collected throughout a growing season can enhance differences in vegetation phenology (Tucker *et al.*, 1985).

In closing, it can be inferred that there is still a need for the development of a relevant and accurate forest cover-type classification system. It's usefulness in sustainable management of forest resources cannot be emphazied. To date, fewer researchers have presented results from the use of actual TM data in forestry applications. Yet out of the regional forest classifications presented, few achieved genus or species level accuracy. On the other hand, mixed results have been achieved with respect to the best season to acquire TM data. In a quest for an answer, this study aims to determine the level of forest categorization that is possible with TM data. It also aims to evaluate TM data from early summer and late-summer for seasonal variablity. Specifically, emphasis is placed on determining which season best captures the differences in leaf phenology. These differences are expected to help in mapping specific forest cover types.

Chapter 3

Materials and Methods

3.1 Study Area

The study area is the Carmanah Valley, located on the West Coast of Vancouver Island, roughly 25 Km north of Port Renfrew (Figure 1). It covers a total area of 6731 hectares and is comprised mainly of Pacific coastal temperate oldgrowth rainforest. One hundred and sixty four hectares at the north of the valley were logged in the late 1980's. The southern end of the valley contains the Carmanah Giant, which at 95m is the worlds tallest sitka spruce (*Picea sitchensis*) (National Geographic, 1997), while the central floodplain is home to groves of other very large sitka spruce (Macmillan Bloedel Ltd, 1989). The valley also contains thousands of hectares of mature western hemlock is (*Tsuga heterophylla*), western redcedar (*Thuja plicata*), and fir (a collection of pacific silver fir (*Abies amabilis*) and other *Abies spp*) mixed in various proportions, with western hemlock being the dominant species in majority of the stands. Several other cover types are also prevalent including juvenile softwood stands on recently cut areas, low density shrub fields, bare ground, swamps, rock outcrops, and lakes.

Study site selection was largely dependent on the diversity of forest cover types, and the availability of satellite data (Landsat TM data) acquired in 1992 and forest cover maps (ground truth data) that have been digitized and archived in a GIS. Another consideration was that collection of ground truthing for old TM data on the Landsat scale is difficult (i.e., it is not possible to reconstruct

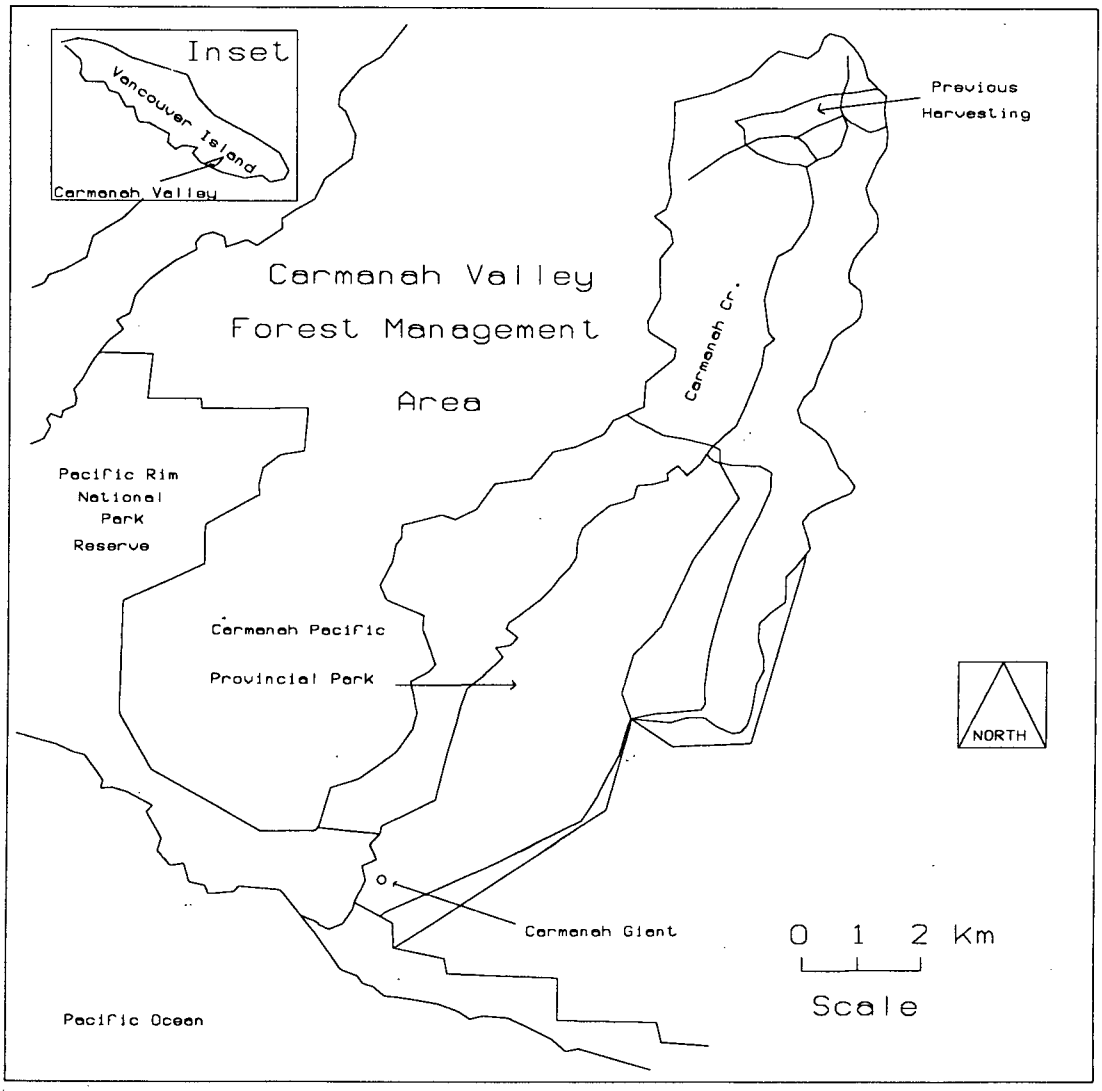

Figure 1. Location of project study area

the events for when the overpass took place). Fortunately enough, because of the valley's uniqueness, logging and other forest disturbances have been prohibited and the area reserved as a park since 1990. Moreover, an oldgrowth rainforest is not expected to change much over roughly a three year period. Additionally the region was under the public eye and as a consequence made more accessible than ever before.

3.2 Satellite data sources

Landsat Thematic Mapper (TM) data of Carmanah Valley and its environs were provided by Radarsat International to UBC forestry for pedagogic purposes. The first Landsat TM scene was imaged on June 30, 1992. Thin cloud, which was not evident in the quick-look images, covered a portion of the study area. The second Landsat TM scene was imaged on September 30, 1992, three months after the first. Unlike the first image, this image was cloud free with satisfactory fidelity and quality (Fig. 2).

3.3 Acquisition of Reference data

Reference data utilized in this study were acquired from different sources, namely Macmillan Bloedel forest cover maps (digital forest cover map and accompanying database), aerial photographs (UBC GIC) and a topographic map (UBC map library). Cover type changes and boundaries were verified or, if necessary, corrected for changes that occurred between Landsat data acquisition and preparation of forest cover maps. Guidelines for defining cover types, as outlined in Eyre (1980), were utilized during the interpretation phase. Forest parameters heavily relied upon for clues for forest cover

Figure 2. 4, 5, 3 False Colour Composite showing entire Scene (a) June, 1992 image with cloud cover depicted as a bluish cast (b) September, 1992 image.

(a)

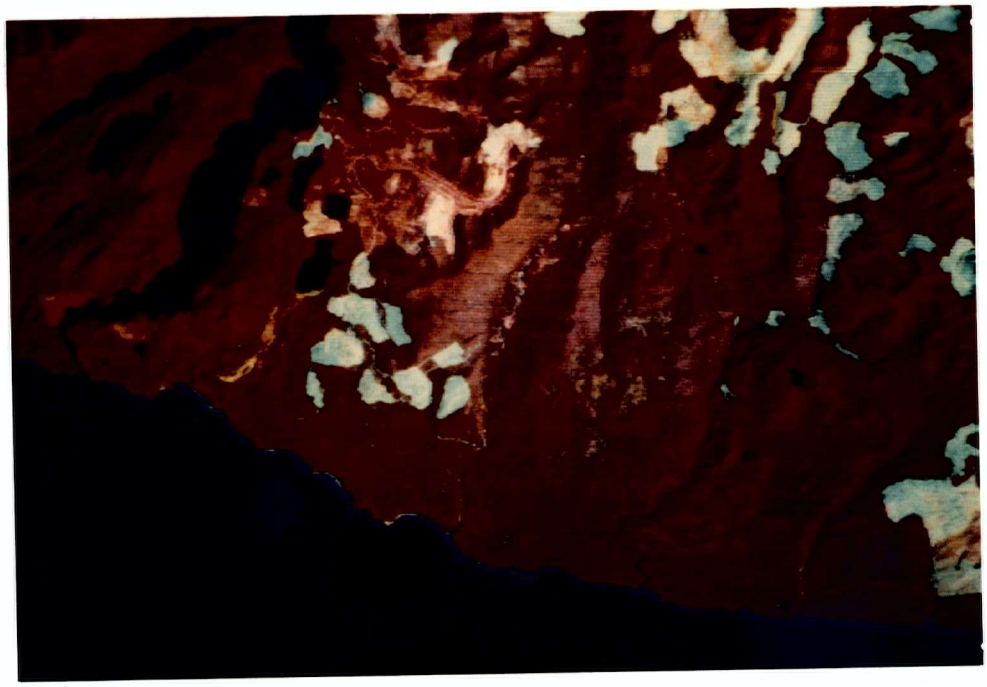

(b)

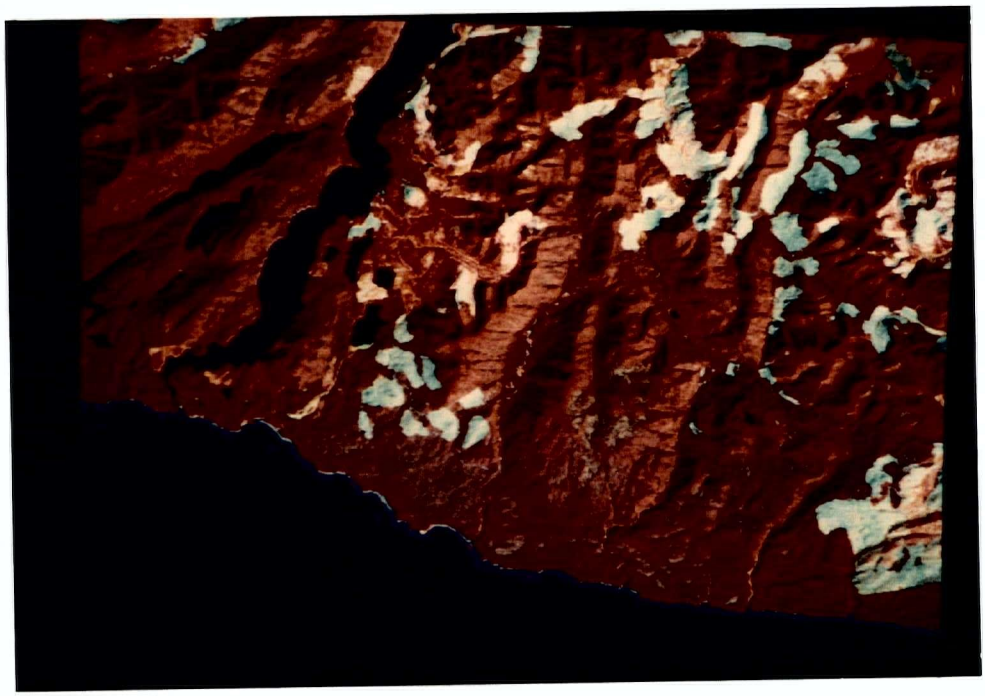

type recognition included species composition, age class and stocking level. Cost constraints coupled with inaccessibility to the vast majority of the stands limited field work to only a reconnaissance survey.

Forest cover-types considered included the following, with their description adopted from Eyre (1980) and their inventory estimates based on the Carmanah Valley management plan (Macmillan Bloedel Ltd, 1989); (A) Sitka spruce comprises about 2% of the stocking of the entire watershed and occurs in combination with western hemlock and western redcedar. It is restricted to a narrow band at low elevations along seaward-facing slopes extending inland a few miles along streams and in most north-facing slopes. Sitka spruce is usually considered a sub-climax species eventually yielding to a western hemlock climax. It is less tolerant of shade than western hemlock. It may behave as a climax species over very long periods on valley bottoms, where seedbeds favour continuation of open stands.

(B) Western hemlock comprises roughly 44% of the stocking. Most common tree associates include sitka spruce, western redcedar and true fir. Western hemlock is generally considered to be a climax type on moist sites, but successional patterns vary with soil type and moisture gradient. Following stand removal, western hemlock may regenerate at once to form pure stands. Western hemlock is a climax species on environmentally moderate sites, but western red-cedar, an important associate, tends to persist as part of the climax forest in wet situations.

(C) Fir comprises 20% of the stocking. Both fir and western hemlock are very shade tolerant and reproduce themselves well under closed canopies, although the fir will usually displace the hemlock in the montane environments generally occupied by this type. This is usually not the case at lower elevations in coastal B.C. Wood productivity ranges widely, depending on soil conditions and temperature regimes.

(D) Western redcedar (WRC) consists of about 30% of the stocking. Major associates include sitka spruce and western hemlock. This type typically occupies moist or wet soils on flats, mountain slopes, and valley bottoms. Old-growth stands typically contain many large trees of advanced age. WRC is usually the most self-regenerating tree in virgin stands of the type. It tolerates high water tables. Although WRC often forms climax stands on wet to very wet sites, it lacks the shade tolerance to become established beneath undisturbed old-growth stands where western hemlock and fir compete.

3.4 Methods

3.4.1 Rectification of Landsat Data

All image processing were carried out in the laboratory of Forest Information Resource Management System (FIRMS) using PC-based PCI software (Version 5.1 EASI/PACE) installed in a Sekani 486/25 computer. The entire scene was first displayed on the RGB monitor (Figure 2). From this display, a 512 by 512 subscene, covering the study area in both the June and September images, was extracted with the aid of reference data.

Geometric distortions were corrected by analyzing well distributed ground control points (GCPs) occurring in the June, 1992 TM image. These were points or features that could be accurately identified on both the topographic map and the image. Features considered for GCPs included forest road intersections, distinct shorelines, clear-cut boundaries, creek and lake edges, and pronounced mountain tops among others. UTM co-ordinates (Easting and Northing) for selected GCPs were read from a topographic map (map sheet No. 92 C/10 and scale 1:50000) and tied to the display. For each GCP entered, its accuracy was assessed based on the root mean square (RMS) error such that those that inflated RMS error were removed.

UTM co-ordinates for 36 GCPs were submitted to a least-squares regression analysis to determine the coefficients for two co-ordinate polynomial transformations that could be used to interrelate the geometrically correct map co-ordinates and the distorted image co-ordinates (EASI/PACE, 1992). The nearest-neighbour resampling technique, in conjunction with a third order of polynomial, were used to correct the image. This option preserved the original input pixel values (DNs). The corrected June image served as a master reference image for rectifying the September, 1992 image, in an image-to-image correction step/tiedown procedure provided by PCI.

3.4.2 TM Dimensionality and Band Reduction

The SAS (SAS Institute Inc., 1988) procedure for principal component analysis (Princomp) was used to compute desired principal components. All six reflective TM bands (bands 1, 2, 3, 4, 5 and 7) were input into the analysis. The procedure first transformed the raw data (DN values) into a correlation matrix. The eigenvalues for this matrix, one for each principal component were then computed. Contribution of each principal component to the total variation was also calculated and arranged from the highest contribution to the lowest. The eigenvectors from each principal component were also calculated. The number of principal components to consider for later digital analysis was selected based on a descriptive rule. The rule adopted was a cumulative proportion of 98% of the total variation.

Highly correlated subsets of bands were grouped with the aid of the correlation matrix. Each distinct group was subjected to a further principal component analysis. From this, the first principal components were considered for visual analysis. Additionally, TM band reduction was performed. The criteria was to select bands with the highest eigenvector coefficient in each distinct group. Selected

bands in combination with TM 4 were used to create a colour composite for visual interpretation and further digital analysis such as training and accuracy assessment.

3.4.3 Spectral Contrast Mapping.

In another run of PCA, only pairs of images of low correlation were used as input variables. By using only two images, two principal components were generated. The first component was discarded because it contained information common to both bands. The second component was examined for spectral contrast among forest cover types. A black and white image of this component was visually analysed and its potential for inclusion in later digital analysis considered.

3.4.4 Classification of Thematic Mapper Data

Both supervised and unsupervised techniques were examined for their utility in subscene classification. In the unsupervised approach, several types of clustering methodologies were tested. Generated spectral classes were identified using reference data.

A traditional approach was utilized in delineating training areas. This involved digitizing training area polygons on the image display of enhanced false colour composites. The digital forest cover map, aerial photographs, topographic map and other auxiliary data served as reference data. For each information class or spectral class, consideration was given to selection of training areas that were representative and evenly distributed throughout the entire image. The aim was to develop sufficient training statistics for all spectral classes constituting each information class so as to improve discrimination by the classifier. However, forest complexity complicated identification and generation of sufficient training areas.

A training set refinement process was performed to check if all data sets were unimodal and spectrally pure. Spectral separability of training areas was evaluated as follows. Training areas that included more than one spectral class were identified and recompiled. Likewise, extraneous pixels were deleted from some of the training data sets. Training areas that might be merged were identified and additional training sets were delineated for poorly represented spectral classes.

In addition to the original TM bands, 1 to 5 and 7, five derivative bands were prepared for spectral analysis and/or band selection. Widening band selection was deemed necessary because of the narrow spectral separation seen between cover types. The first derivative band was a principal component analysis of visible bands. Other derivative bands included image ratios. Band ratios 4/3 and 5/4 have been shown to be sensitive to changes in vegetation characteristics (Peterson *et al.*, 1986). Jensen (1983), among others, reported that TM4/TM3 provides information with respect to vegetation and canopy condition and that TM5/TM2 may be a promising feature for wetland identification. NDVI was prepared mainly to assist in studying stand biomass levels. Finally, spectral pattern analysis was performed on all possible bands in an attempt to select an optimum band combination for supervised classification.

The classification algorithm utilized was a maximum-likelihood classifier (MLC). The main advantage of the MLC is that it takes the variability of spectral classes into account by using the covariance matrices of these classes. It quantitatively evaluates both the variance and correlation of the category spectral response patterns when classifying an unknown pixel (Lilesand and Kiefer, 1994).

Two iterations of a mode filter rule (FMO) smoothing, using a 3 by 3 window, were applied to the final classified image (thematic map) prior to accuracy assessment. The majority class within the window was first determined. If the center pixel happened to be not the majority class, its identity was

changed to the majority class. As the window progressed through the data set, the original class codes were continually used, not the labels as modified from the previous window positions.

3.4.5 Classification Accuracy Assessment

Accuracy assessment is an essential component of the classification process. A complete assessment was performed for all three classification results. Test areas were located with the aid of forest cover maps, aerial photographs and a topographic map. The guiding rule was to delineate areas that were representative and different from, and considerably more extensive than, training areas. Some sections of training data polygons were utilized to perform accuracy assessment. From test areas, the known category type of pixels were listed versus the classified categories. This represented a contingency table or error matrix. Based on this table, classification accuracy (total percent correct) was computed. Average classification accuracies for the June, September and multitemporal TM dataset were then subjected to analysis of variance to determine if they were significantly different. Scheffe's multiple range test was used to perform pairwise comparisons.

3.4.6 Extraction of Representative Sites

From geocoded images, matching 512 by 512 subscenes covering the study area in both June and September were extracted. Representative samples for the study of stand age and density were drawn from mixed cedar and hemlock stands. The choice of this stand type was based on the fact that it contained all desired age and stocking level stratifications. Numeric image window (NUM) command in PCI was used to generate DNs for each selected sample site. Recorded digital values from both original and derivative bands were then arranged in a spreadsheet before entering them into the SAS

statistical program. Descriptive statistics including means, variances, coefficient of variation, minimum and maximum values, histograms, skewness and kurtosis were computed. Additional analyses included generating and evaluating covariance and correlation matrices. Analysis of summary statistical measures provided an overview of the distribution of DNs by band of the multitemporal TM spectral data and, most importantly indicated the separability between forest-cover types and their characteristics. Illustration of separability between cover types was further improved by graphic presentation of mean DNs versus bands for all cover types and forest parameters considered.

3.4.7 Change Detection

Image differencing, image ratioing, and the normalized difference vegetation index (NDVI) were three image digital change detection techniques utilized in this study. In image differencing, the spatially registered images of June and September were subtracted band by band in order to produce a further image which represented change. Mathematically:

$$Dx = x(t1) - x(t2) + C$$

where Dx is the difference in pixel value, x is the pixel value for band k and t1 = first date (June, 1992), t2 = second date (September, 1992) and C is a constant added to produce positive digital numbers. A threshold boundary between change and no-change pixels was selected based on standard deviations from the mean pixel value.

Ratioing is considered to be a rapid means of identifying change. The registered image of June, 1992 was divided by the registered image of September 1992 on a band by band basis. Ratio computation was as follows:

$$Rx = x(t1) / x(t2)$$

where Rx is the ratioed pixel value and x, t1 and t2 are as defined above.

In vegetation studies, ratios, commonly known as vegetation indices, have been developed for the enhancement of spectral differences on the basis of strong vegetation absorbance in the red and strong reflectance in the near-infrared part of the spectrum (Singh, 1989). NDVI, demonstrated in many studies to be significantly related to green leaf biomass, was computed for each image as follows:

$$NDVI = (TM4 - TM3) / (TM4 + TM3)$$

where TM3 and TM4 correspond to digital numbers in TM bands 3 and 4 respectively. The difference between the NDVI for June and September was evaluated to determine whether or not the forest canopy had been altered.

Chapter 4

Results and Discussion

4.1 Spatial Calibration and Geocoding

The aim of image rectification and restoration was to first correct the image data for distortions and degradation's stemming from the image acquisition process (Lillesand and Kiefer, 1994) and secondly to allow for relatively easy overlay of reference data sets for training and accuracy assessment later on. Lack of information on solar angle among other parameters limited radiometric calibration.

The June TM image was geometrically registered to the UTM zone 11 co-ordinates with a pixel size of 25 metres using nearest-neighbour resampling and a third order polynomial transformation. The nearest-neighbour resampling technique was chosen in an attempt to preserve the original digital numbers. A total of 36 GCPs was used to register the image. Refer to Appendix 1 for a list of GCPs ordered from the worst to the best residuals and the results of least-squares regression analysis for the two co-ordinate transformation. A root mean square error of 0.40 was achieved for the fitted polynomial regression model.

The registered June TM image was utilized in an image-to-image resampling technique to correct the September image. Geocoded images are presented in Figures 3a and 3b.

4.2 Spectral Attributes of TM Data

Descriptive statistics of multitemporal TM data (mean, standard deviation, minimum and maximum digital numbers (DN)) for the two dates were computed and compared band by band. They

Figure 3. Geocoded Thematic Mapper images showing (a) June, 1992 subscene and (b) September, 1992 subscene covering study area.

(a)

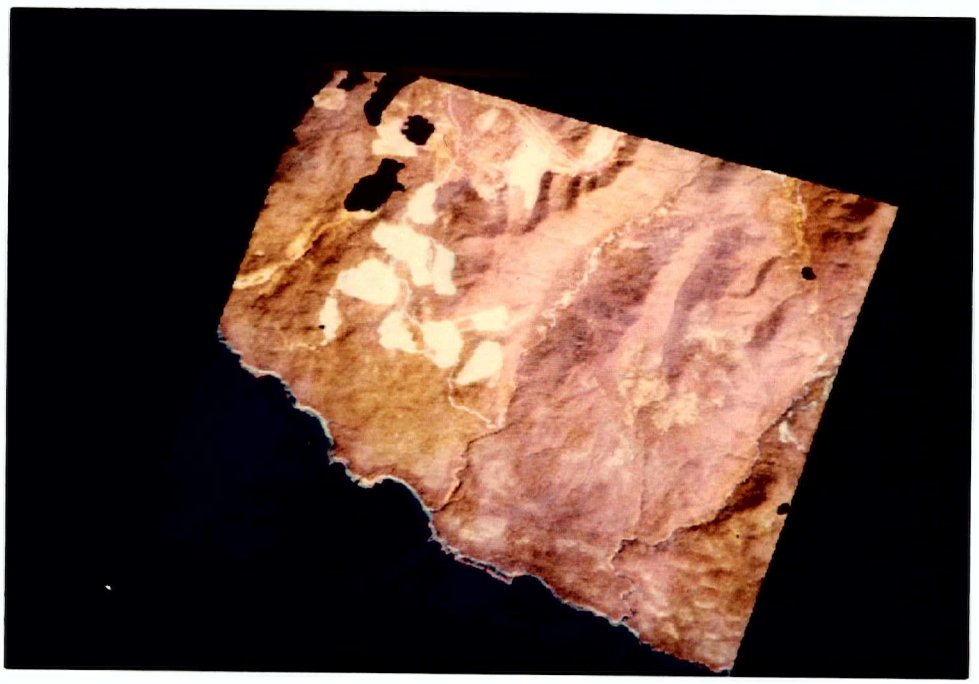

(b)

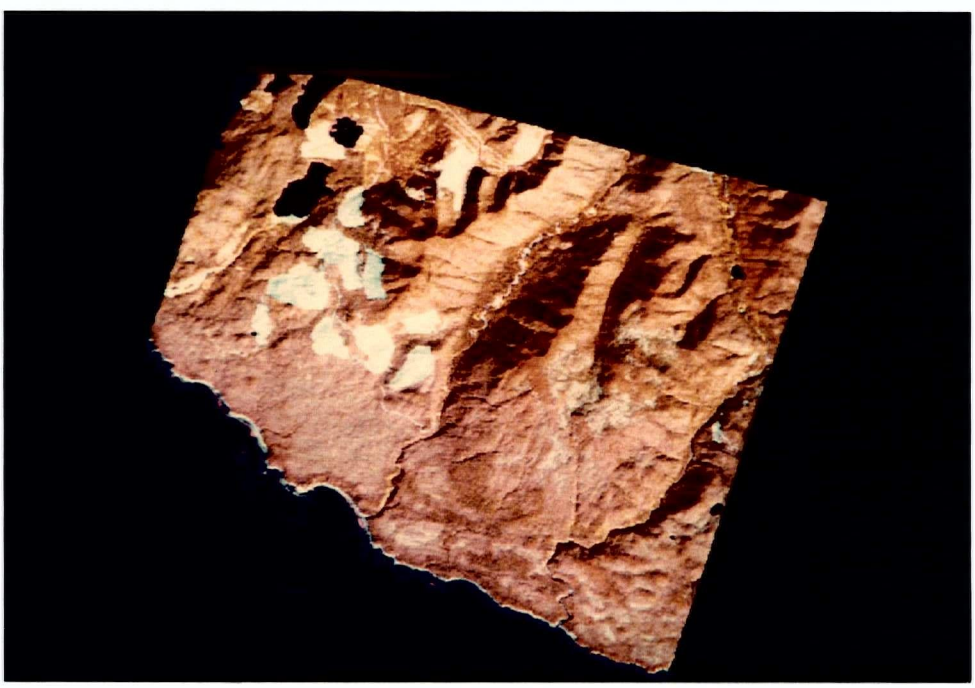

are given in Table 2. The distribution of mean digital values from the scenes in June and September is best illustrated in Figure 4. Except for the thermal infrared band (band 6), mean digital numbers values for June were generally higher than for September. This can be attributed to the solar angle with the sun being at it's zenith in June and away from this position in September. Generally, the dynamic range occupied by both datasets is small in relation to the 256 levels available. However, the September image utilized a wider range than June image.

4.3 TM Dimensionality and Band Reduction

A summary of standard principal component analysis results are presented in Tables 3a and 3b. Correlation matrices indicated that the September image had a slightly higher correlation between visible bands than the June image. Band 1 versus band 2 correlation was 0.7282 and 0.8482 in June and September respectively. Band 1 versus band 3 correlation was 0.7779 in June but 0.8305 in September. The correlation seen between TM band 1 and the other visible bands in the June image could be related to haze and cloudy conditions present at the time of image acquisition. The blue band was likely more scattered than the green and red bands. Band 2 and band 3 were highly correlated for both dates (0.9218 in June and 0.94 in September). Band 1 was less correlated with the infrared bands than were the other two visible bands. Bands 2 and 3 were highly correlated to band 7 (0.8157 and 0.8690) in June and band 3 moderately correlated to band 7 (0.7605) in September. Additionally, eigenvalues and eigenvectors were analysed. Table 4 summarizes the results. The first three principal components (Figures 5 and 6) explained 97.63 and 97.60 percent of the image information in the June and September TM data, respectively. In each case, the first two principal components had an eigenvalue greater than one. These two components could suffice for dimensional reduction,

Table 2. Descriptive statistics of TM data

	June, 1992 TM data				September, 1992 TM data			
Band	Mean	Std	Min	Max	Mean	Std	Min	Max
1	90.33	5.19	2	201	59.83	5.56	49	250
2	34.97	3.42	26	91	20.59	3.42	13	122
3	35.55	5.06	24	107	18.04	5.29	8	168
4	60.82	19.44	10	139	41.07	19.28	1	125
5	43.44	15.57	10	149	24.95	15.24	0	156
6	98.90	6.08	78	122	110.33	2.83	104	127
7	15.35	6.07	3	66	7.27	5.73	0	69

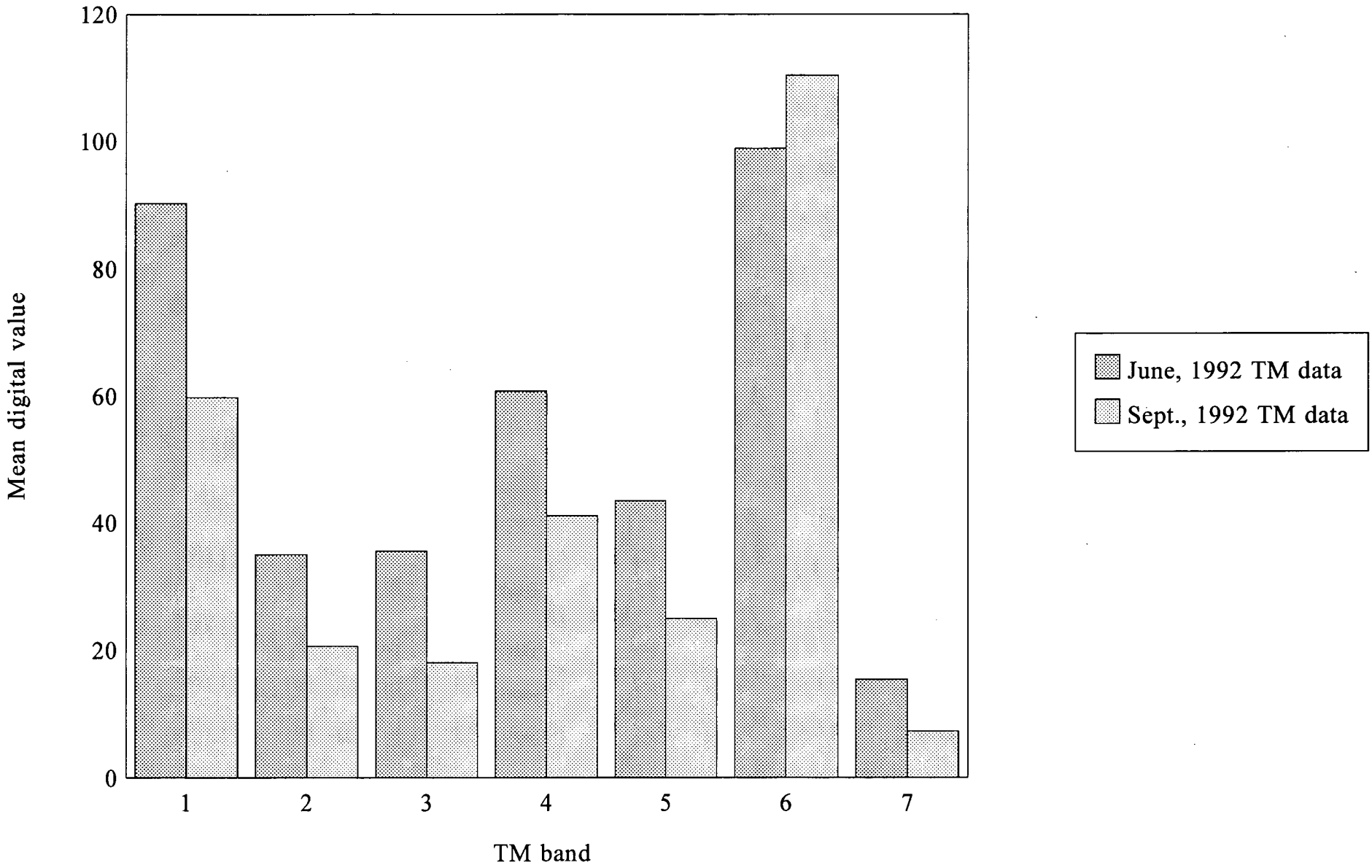

Figure 4. Mean digital values for June and September TM data.

Table 3a Correlation matrix for June TM data

	Band 61	Band 62	Band 63	Band 64	Band 65
Band 61					
Band 62	0.7282				
Band 63	0.7779	0.9218			
Band 64	0.0517	0.6197	0.4949		
Band 65	0.3693	0.7982	0.7975	0.8034	
Band 67	0.5351	0.8157	0.8690	0.6050	0.9363

Table 3b Correlation matrix for September data

	Band 91	Band 92	Band 93	Band 94	Band 95
Band 91					
Band 92	0.8482				
Band 93	0.8305	0.9400			
Band 94	0.0574	0.4386	0.4242		
Band 95	0.3563	0.6423	0.7142	0.7748	
Band 97	0.4651	0.6643	0.7605	0.5748	0.9388

Band 61, 62, ..., 67 - TM band , 1, 2, ..., 7 acquired in June, 1992.

Band 91, 92, ..., 97 - TM band 1, 2, ..., 7 acquired in September, 1992.

but to avoid the risk of leaving out crucial information, the third principal component was included in later analyses. This component explained 4.68 percent and 6.12 percent of the variation in June and September TM data, respectively. The fourth, fifth and sixth principal components collectively accounted for 2.37 percent of the image information in the June scene and 3.4 percent of the image information in the September scene. The compression of image information in the first three principal components is typical of Landsat TM data, where the intrinsic dimensionality is three. These components were visually analysed and preserved for supervised classification and change detection. In this context, the transformed data reduced the number of computations required, as illustrated later, and as such made the classification process much more efficient.

4.4 Selective PCA for TM Band Selection

Visible, near-infrared and mid-infrared wavelengths occupy three fundamentally independent spectral regions. Subsets of highly correlated groups of bands (TM bands 1, 2 and 3 on the one hand and 5 and 7 on the other) served as input in selective principal component analysis. The idea was to select a representative band in each subset to be combined with TM band 4 in colour compositing for visual analysis. A summary of the PCA analyses are presented in Tables 5a and 5b. PC1 in the visible region accounted for 87.38 percent and 91.56 percent of the image information in the June and September TM data respectively. Based on a cut-off eigenvalue of ≥ 1, PC1 qualified for further analysis in band reduction. However, a substantial amount of variation, 10 percent (June scene) and 6 percent (September scene) were left over in PC2.

Figure 5. Transformed data resulting from PCA of June data. The percentage of image information contained in the first three principal components is distributed as indicated.

(a) PC1, 74.37%

(b) PC2, 18.58%

c) PC3,

4.68%

PC3 shows distribution of cloud cover.

Figure 6. Transformed data resulting from PCA of September TM data. The percentage of image information contained in the first three principal components is distributed as indicated.

(a) PC1,

70.25%

(b) PC2,

21.23%

(c) PC3,

6.12%

PC3 image shows image stripping.

Band selection was based on the eigenvector loadings. The magnitude of each coefficient of the eigenvectors showed the importance and correlation of each spectral band to the corresponding principal component. All visible bands were moderately related to PC1 for both dates. In the June TM data, band 3 was more highly related to PC1 than either band 1 or 2; thus, band 3 was found to be a suitable representative for the visible region. In relative terms, bands 2 and 3 in the September TM data were more highly related to PC1 than band 1 and, as a consequence, both qualified for inclusion in a composite prepared for visual analysis. Band 3 may have an edge over band 2 since it is less affected by atmospheric scattering.

Mid-infrared band selection was achieved using PCA results summarized in Table 5(b). PC1 accounted for 96.81 percent and 96.94 percent of the image information in the June and September TM data, respectively. This constitutes a large amount of total scene variation. Variation left over in PC2 may be mostly system noise. Based on an eigenvalue ≥ 1 as the criteria for selection, only PC1 met this criteria. Inspection of the eigenvector loadings revealed that bands 5 and 7 in both the June and September TM data were highly correlated to PC1. Both bands were thus important in explaining image information and/or scene variation acquired in the mid-infrared region. PCA may not be sufficient for band selection in this spectral region. However, band 5 was selected based on descriptive statistics in Table 2 (see page 32) which showed that it covered a wider range of the radiometric levels (10-149 and 0-156) and lower coefficient of variation than band 7. In combination with TM band 3 (visible) and TM band 4 (near-infrared) a false colour composite (Figures 2 -see page 20) was derived which is in agreement with Horler and Ahern's (1986) suggestion that TM bands 3, 4 and 5 are best suited for producing enhanced colour imagery for most forestry applications. Another enhanced colour composite was created using PC1 (visible region), PC1 (mid-infrared) and TM band 4 (Figures

Table 4. PC's Eigenvalues and variation accounted (six reflective TM bands)

	June, 1992		September, 1992	
Principal Component	Eigenvalue	Proportion of Variation	Eigenvalue	Proportion of Variation
1	4.4624	0.7437	4.2150	0.7025
2	1.1149	0.1858	1.2740	0.2123
3	0.2809	0.0468	0.3669	0.0612
4	0.0726	0.0121	0.0785	0.0131
5	0. 0500	0.0083	0.0444	0.0074
6	0.0194	0.0032	0.0211	0.0035

Table 5a. PC's Eigenvalues, variation accounted and eigenvetors (TM visible bands)

	June, 1992 TM data			September, 1992 TM data		
Principal component	Eigenvalue	Proportion of variation	Eigenvectors	Eigenvalue	Proportion of variation	Eigenvectors
1	2.6215	0.8738	0.55,0.59,0.60	2.7467	0.9156	0.56,0.58,0.58
2	0.3043	0.1014	0.83,-0.48,-0.29	0.1941	0.0647	0.82,-0.34,-0.45
3	0.0742	0.0247	0.11,0.66,-0.75	0.0591	0.0197	0.07,-0.73,0.68

Table 5b. PC's Eigenvalues, variation accounted and eigenvectors (TM shortwave-infrared)

	June, 1992 TM data			September, 1992 TM data		
Principal component	Eigenvalue	Proportion of variation	Eigenvectors	Eigenvalue	Proportion of variation	Eigenvectors
1	1.9363	0.9681	0.71, 0.71	1.9389	0.9694	0.71, 0.71
2	0.0637	0.0319	0.71,-0.71	0.0611	0.0306	0.71,-0.71

7a and 7b). Statistically and visually, this composite contained a vast amount of image variation and highlighted several cover types and features.

4.5 Spectral Contrast Mapping of Multitemporal TM Data

Multitemporal TM data were created by combining the geocoded TM data acquired in June and September into one image file in PCI. Principal component analysis was conducted on these data in an attempt to map the spectral contrast between the two datasets. A summary of the correlation between reflective TM bands in June (6) and September (9) is presented in Table 6. The following pairs of TM bands were established to be highly correlated: band 64 (June and TM4) and band 94 (September and TM4); band 65 and band 95; band 65 and band 97; band 67 and band 95; and band 67 band 97. It is evident that high correlation was seen between bands covering the same spectral region, mainly near-infrared and mid-infrared. Moderate correlation was seen between numerous pairs of bands. These included: band 62 and band 93; band 62 and band 95; band 62 and band 97; band 63 and band 93; band 63 and band 95; band 63 and band 97; band 64 and band 95; band 65 and band 93; band 65 and band 94; and band 67 and band 93.

The first six principal components accounted for approximately 98.09 percent of the image information (Table 7). This is enough variation to warrant exclusion of the remaining principal component from further analysis. Selection of TM bands for visual analysis was based on the eigenvector loadings. None of the 12 TM bands were highly related to PC1. TM bands 61, 63, 91, 92, 94 and 97 were related to the other components . This was found to be a wide selection given the three band limit in colour compositing (composite). From visual inspection, bands

Figure 7. Intensity, Hue and Saturation (IHS) enhancement of PC1 (visible region), TM4 and PC1 (short-wave-infrared region). (a) Enhanced June, 1992 composite. Black is water and shadows, yellow is mixed hemlock and cedar stands, blue is alpine conifers, regenerating stands and mixed spruce/hemlock stand, cyan is scrubland, purple is sunlit conifers, grayish blue-violet is clearcuts and, green, red and orange are other mixed forest covertypes. (b) Enhanced September, 1992 composite. Black is water and shadows, cyan is scrubland, swamps and mixed hemlock and cedar stand, yellow is mixed cedar/hemlock and hemlock/cedar/fir stands, purple is alpine conifers, red is mixed spruce/hemlock stands and other forest stands and deep bluish violet is clearcuts.

(a)

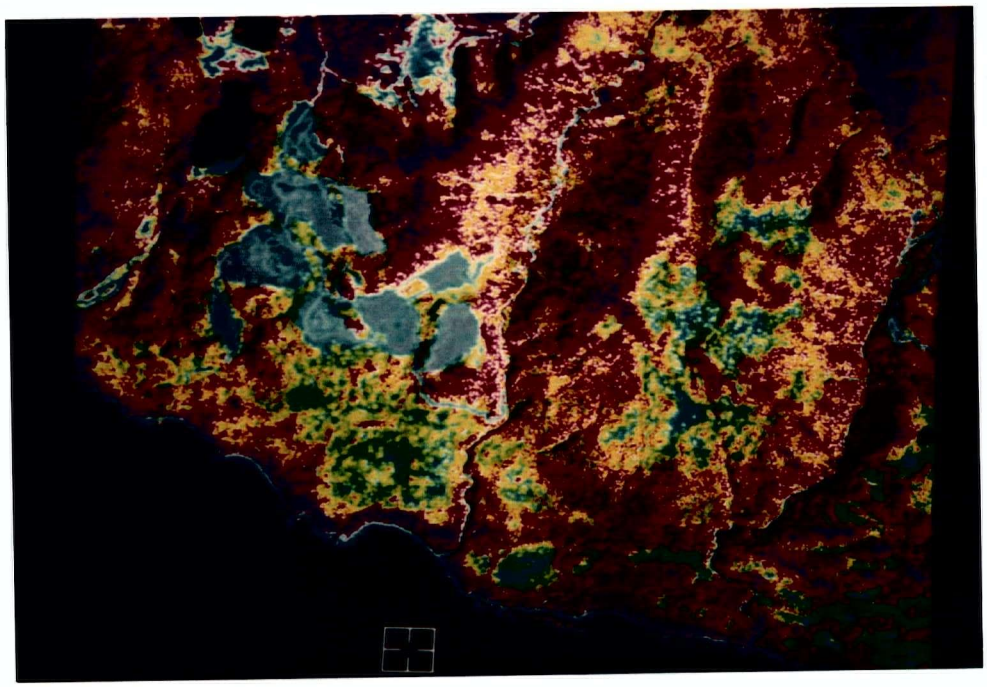

(b)

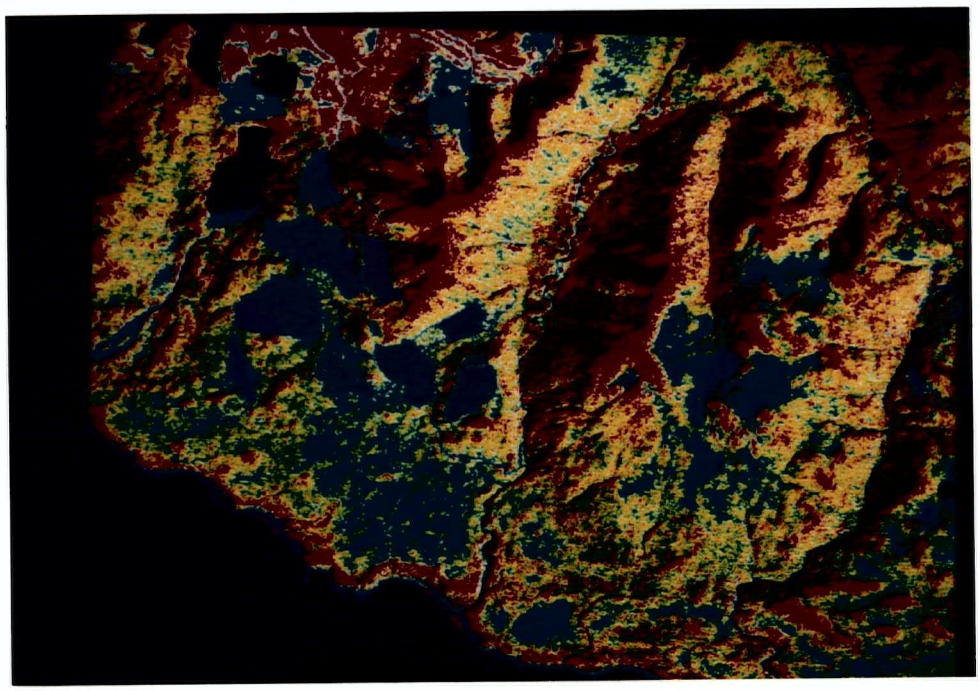

Table 6. Correlation matrix for Multitemporal TM data

	Band 61	Band 62	Band 63	Band 64	Band 65	Band 67
Band 91	0.5023	0.4029	0.4579	-0.0360	0.2637	0.3897
Band 92	0.4387	0.5995	0.5995	0.3402	0.5499	0.5851
Band 93	0.4916	0.6598	0.6973	0.3674	0.6481	0.7005
Band 94	0.0164	0.5549	0.4233	0.9209	0.7190	0.5284
Band 95	0.3185	0.7307	0.7186	0.7490	0.9296	0.8726
Band 97	0.4305	0.7192	0.7626	0.5650	0.8822	0.9017

Table 7. Multitemporal Eigenvalue and variation accounted

Principal Component	Eigenvalue	Proportion of Variation
1	7.8632	0.6553
2	2.0510	0.1709
3	1.1051	0.0921
4	0.5096	0.0425
5	0.1565	0.0130
6	0.0848	0.0071

Table 8. Correlation and Spectral Contrast

TM band pair	Correlation coefficient	Principal component 1 variance (%)	Principal component 2 variance (%)
Band 61 and band 94	0.0164	50.8	49.2
Band 63 and band 94	0.4233	71.2	28.8
Band 64 and band 91	-0.0360	51.8	48.2
Band 64 and band 92	0.3402	67	33
Band 61 and band 95	0.3185	65.9	34.1
Band 65 and band 91	0.2637	63.2	36.8
Band 67 and band 91	0.3897	69.5	30.5
Band 62 and band 91	0.4029	70.1	29.9
Band 64 and band 97	0.5650	78.2	21.8

63, 94 and 97 turned out to the best false colour composite. As demand necessitated, other band combinations were chosen. The primary interest in spectral contrast mapping was to enhance the capability of the multitemporal TM data in forest cover discrimination. Based on the correlation matrix in Table 6, the following pairs of bands were found to have low correlation. These included:

(1) band 61 and band 94 (blue and near-infrared)

(2) band 63 and band 94 (red and near-infrared)

(3) band 64 and band 91 (near-infrared and blue)

(4) band 64 and band 92 (near-infrared and green)

(5) band 61 and band 95 (blue and SWIR-1)

(6) band 65 and band 91 (SWIR-1 and blue)

(7) band 67 and band 91 (SWIR-2 and blue)

(8) band 62 and band 91 (green and blue)

(9) band 64 and band 97 (near-infrared and SWIR-2)

The first four pairs were selected to map the spectral contrast between the visible and near-infrared spectral regions. The next three pairs mapped the contrast between the visible and shortwave-infrared regions while the eighth was selected to map the spectral contrast of two bands which are adjacent to each other in the visible spectral region. The ninth pair, whose PC2 image is presented in Figures 8a and 8b, mapped contrast between near-infrared and mid-infrared. Apart from mapping spectral contrast between major spectral regions, these pairs also mapped temporal change.

A relation was seen between band correlation and spectral contrast. The lower the correlation between two input images, the higher the percent of variance that was mapped to PC2, which indicates a larger amount of spectral contrast. In Table 8 for example, TM band 61 and band 94 had a

correlation coefficient of 0.0164 and 49.2 percent of total variance was mapped to PC2. On the other hand, TM band 63 and band 94 had a correlation coefficient of 0.4233 and only 28.8 percent of total variance was mapped to PC2.

4.6 Landsat TM Classification Results

4.6.1 Spectral Clustering and Class Separability

The multitemporal TM datasets were first subjected to spectral clustering (i.e. unsupervised classification). This step provided an opportunity for determining the degree to which forest types could be distinguished and the nature of spectral variability of cover types under study. A total of 20 spectral classes (Figures 9a and 9b) were generated using the K-means clustering technique. The spectral classes included conifers on flat topography, shaded mountain slope conifers, alpine, regenerating conifers, and sunlit mountain slope conifers. Classification of sunlit and shadowed slopes as distinct and separate spectral classes illustrated that topography influenced spectral reflectance of cover types to a great extent. This observation, and clues to possible cover types and location of clearcuts and regenerations, were useful information during the training stage that ensued.

The guiding principle during the training stage was selection and delineation of areas for each information class that were both representative and evenly distributed over the entire image. A total of 18 training areas were delineated in the June image, 17 in the September image and 18 in the multitemporal TM data. The extra class in the June image was clouds which could not be avoided since a satisfactory separation was desired. The composition of the training sites included 12 forest classes, with the rest being other vegetation classes and cultural features.

Signatures generated for each training site were used to compare between each pair of classes.

Figure 8. Results of spectral contrast mapping of TM bands 64 and 97. Alpine/sunlit conifers and regenerating stands are bright toned; cutblocks, creeks, logging roads, swamps, scrub and shoreline are dark toned; water bodies and majority of forest cover types appear in light to moderate tones. (a) June, 1992 black and white PC2 image (b) September, 1992 black and white PC2 image.

(a)

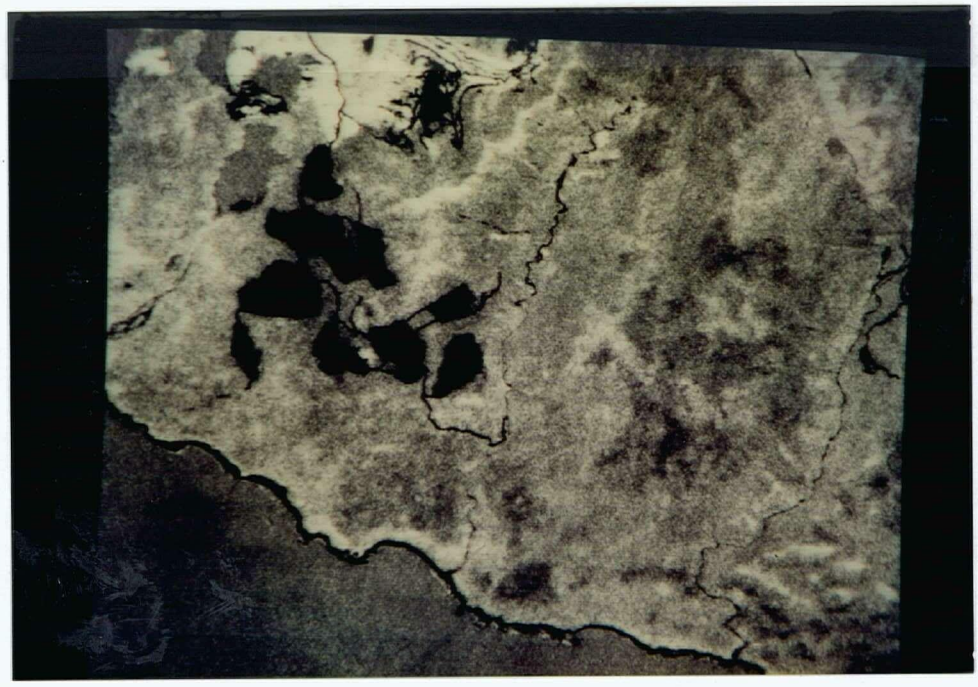

(b)

Figure 9. K-CLUS spectral clusters in TM data. (a) June, 1992 spectral classes. Green is mixed conifers on even/flat topography, blue is conifers on north-facing slopes, yellow is alpine conifers and regeneration stands, pink is upland ('sunlit') conifers, orange is water, red is clouds (over ocean), gray is scrub land, cutblocks and other forest types. (b) September, 1992 spectral classes. Gray is water bodies, green is conifers on north-facing slopes, yellow is upland conifers, regenerating stands and other mixed conifer stands, orange, pale gray and blue are conifer stands containing cedar/hemlock/spruce/fir in various proportions, bluish gray is old clearcuts and light green is new clearcuts.

(a)

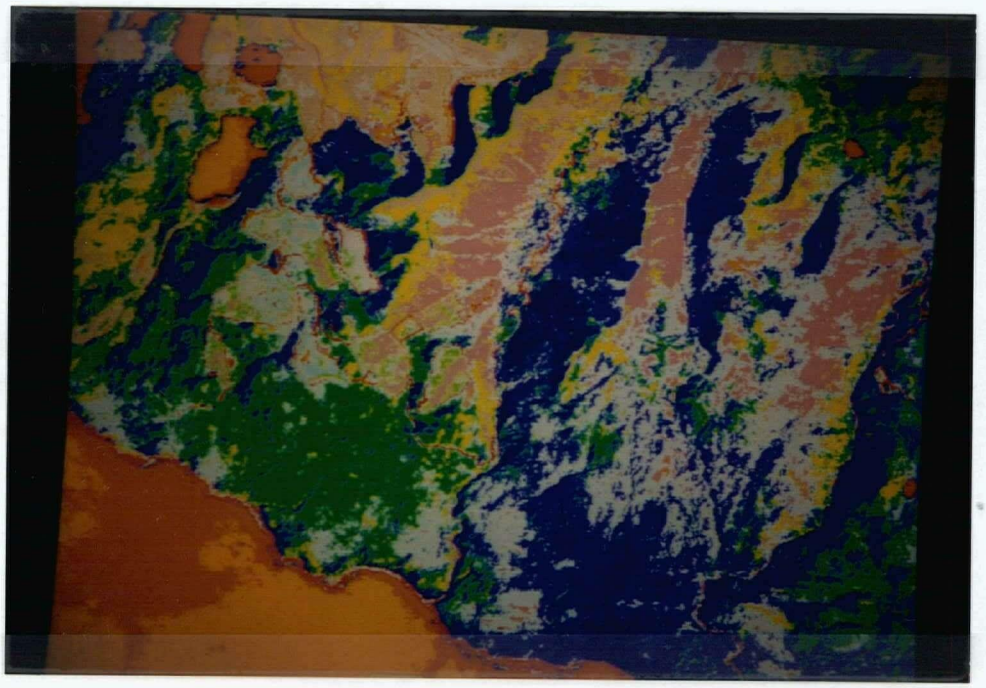

(b)

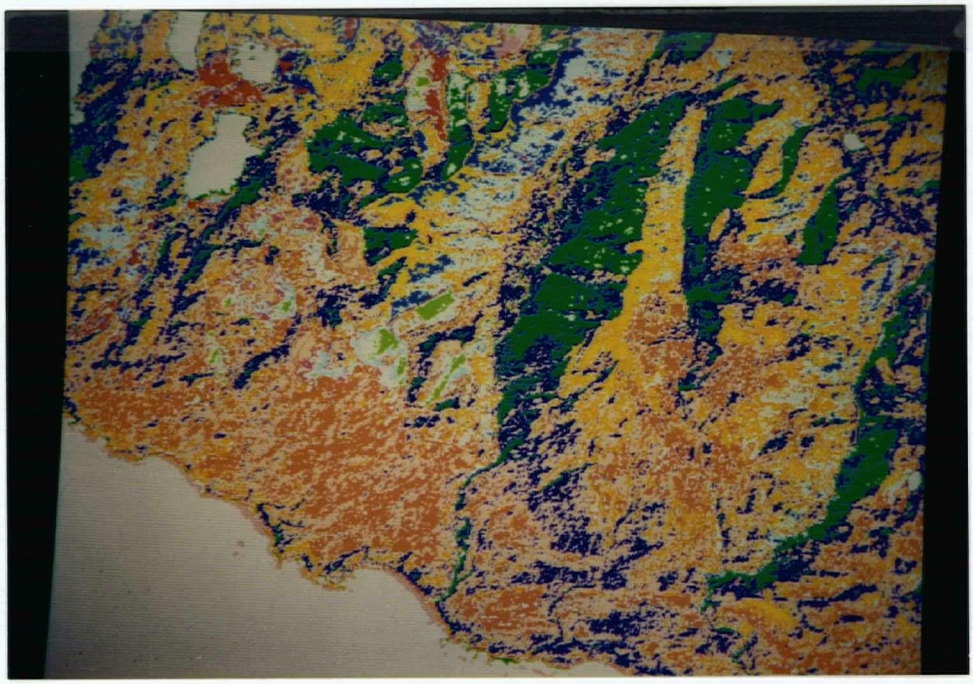

SIGSEP, a signature separability command provided by PCI, calculated statistical and response patterns among trained classes. Transformed divergence served as the separability measure. Divergence matrices for June and September are given in Appendix II. Real values between 0 and 2 were generated. 0 indicated a complete overlap between signatures and 2 indicated a complete separation between any two classes. A value below 1.5 indicated spectrally similar classes. Classes with at least 1.5 and above were statistically separable. In the June TM data, all forest cover types were statistically separable except for juvenile and alpine conifers (1.23), and the conifers on north-facing slopes and densely stocked mixed cedar/hemlock stands (1.25). Juvenile and alpine conifers (1.42), mixed cedar/hemlock/fir stand and spruce/hemlock stand (1.12) on the one hand and dense cedar/hemlock stands (1.34) on the other hand showed poor separability in the September TM data. The rest of the cover types were separable. Nevertheless, it should be noted that, except for a few classes, the training stage was repeated at least three times before the final training set was achieved.

4.6.2 TM and Derivative Band Selection

Two spectral analysis techniques were employed in the selection of band combinations that could best discriminate among forest cover types. The technique involved plotting spectral patterns for all classes (Figures 10a and 10b). Each plot was visually examined for bands or combinations of bands which maximised separability. A limitation of this technique was that there was no indication as to whether separability was improved with the addition or subtraction of bands. A more robust method was based on divergence of signature segments. The CHNSEL (channel selection) command in PCI offers the average interclass divergence, the average transformed divergence and the minimum pairwise divergence as decision rules for computing the dissimilarity between any two signature classes. The first two rules produced similar results. Six out of a possible 12 bands were determined to be the

optimum channel combination for discriminating the set of classes in both dates. The addition of a seventh band did not improve the forest class separability of any of the imagery, while using only five or four bands resulted in a significant loss of both forest class separability and classification accuracy. As in PCA, spectral pattern analysis indicated that the original TM bands 3, 4, and 5 were valuable for forest cover-type classification. Derivative bands were also included in the optimum band combination. For the June TM data, the optimum set of bands included 3, 4, 5, PC1(visible bands), NDVI and 4/3, whereas for the September TM data bands 3, 4, 5, PC1(visible bands), NDVI and 5/4 first were selected as the best combination. It is evident that a similar set of bands were selected for both dates except for image ratios (4/3 and 5/4). For the multitemporal TM data, the two sets of band combinations (i.e., a total of 12 bands) were used. The object in this classification was to utilise scene information from both dates, though at the expense of computing time.

4.6.3 Maximum-Likelihood Classification Results

All three images were classified in PCI using the maximum likelihood classifier (MLC) command. A set of 18 , 17 and 18 signatures in the June, September and multitemporal images, respectively, were used during classification. The final thematic maps were prepared by passing two iterations of a 3 by 3 mode filter on the raw classified image. With two iterations, the "salt and pepper" or noisy pixels were removed. The results are as shown in Figures 11a, 11b and 11c. Cover types included water, clouds, shoreline, mixed cedar/hemlock stands of normal stocking, upland conifers, mixed spruce/hemlock, mixed cedar/hemlock/fir, conifers on north-facing slopes, young (new and old regeneration), alpine conifers, densely stocked cedar and hemlock stands, scrub stand, new clearcuts, old clearcuts, creeks and the void of shadows. A visual analysis of the three maps showed that similar

classification of the Carmanah cover types was achieved. Quantitatively, these thematic maps were of different accuracies. Error matrices for the classification of the June, September and multitemporal TM dataset are summarized in Tables 9a, 9b and 9c. Diagonal elements correspond to correct classification, whereas off-diagonals are misclassifications. Classification accuracy was computed using column totals. Overall accuracies were 79.2 percent (June), 82.2 percent (September) and 90.3 percent (multitemporal), and average user's accuracies were 72.2 percent (June), 78.69 percent (September) and 84.6 percent (multitemporal). Average producer's accuracies on the other hand were 76.9 percent for June, 82.5 percent for September and 91.2 percent for the multitemporal TM dataset.

Classification results, mainly producer's accuracies, achieved using the three datasets are summarized and compared in Figure 12. Generally, the multitemporal TM dataset provided the highest classification accuracy level for most cover types and June had the lowest classification accuracy level in a number of cases. Specifically, all cover types except conifers on north-facing slopes and densely stocked mixed stands of cedar and hemlock were best classified using multitemporal TM data. Between dates, the September scene generally produced a higher classification accuracy than the June image. However a better classification for old clearcuts was achieved with the June TM data than with September data (i.e. 95.53 percent compared to 86.88 percent).

Analysis of variance results for the three average classification accuracies, as presented in Appendix IV, indicated that the three averages were significantly different. In the next step, Scheffe's procedure (SAS Institute Inc., 1988) was used to perform a pairwise comparison of the averages. The alpha level was set at 0.05. Results of the tests are in Tables 10a and 10b. It can be seen that for general cover type classification, the multitemporal dataset was not significantly different from the September dataset but significantly different from the June dataset. Neither the June nor the September

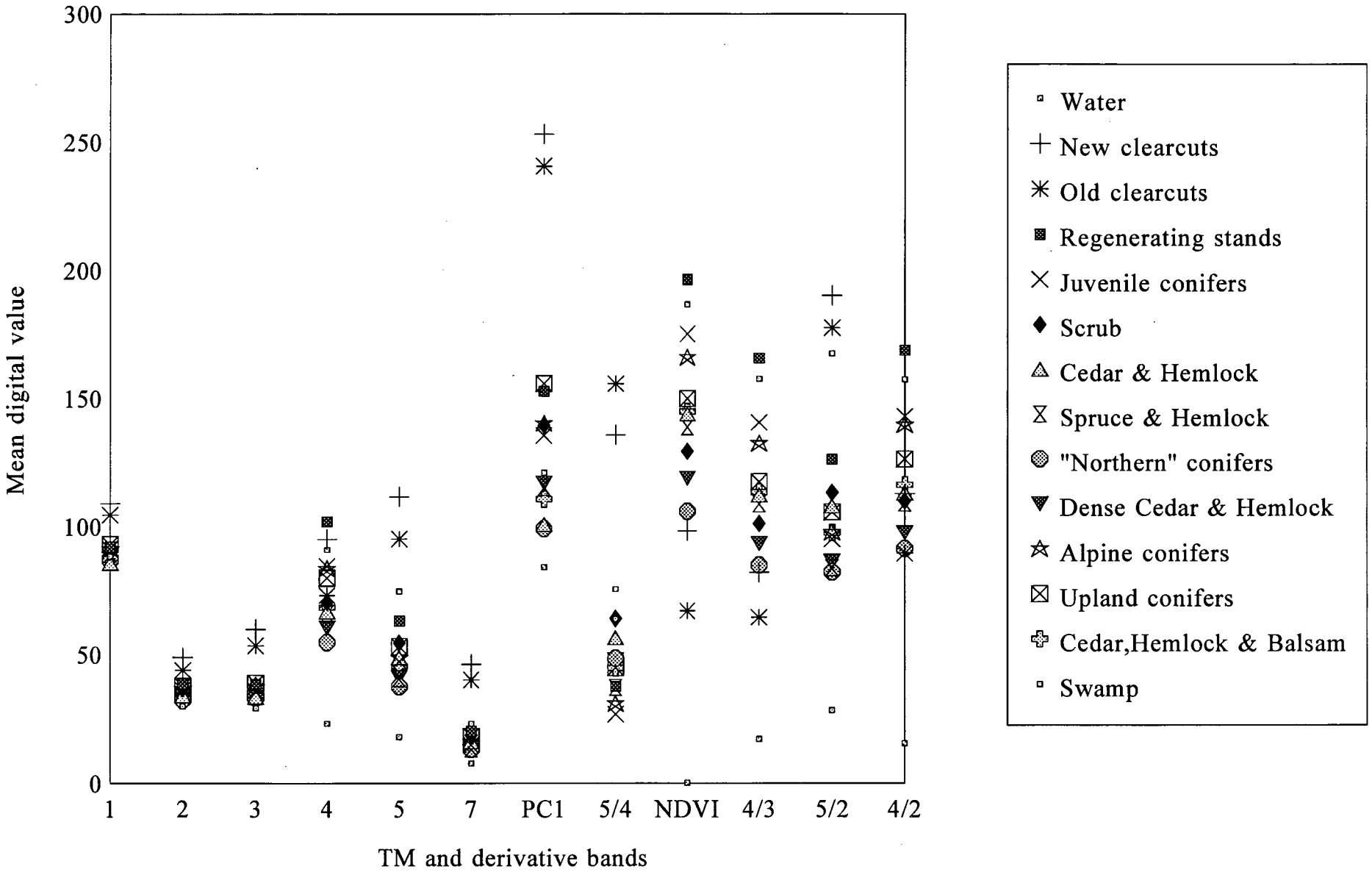

Figure 10a. June spectral pattern plots for cover-type classes.

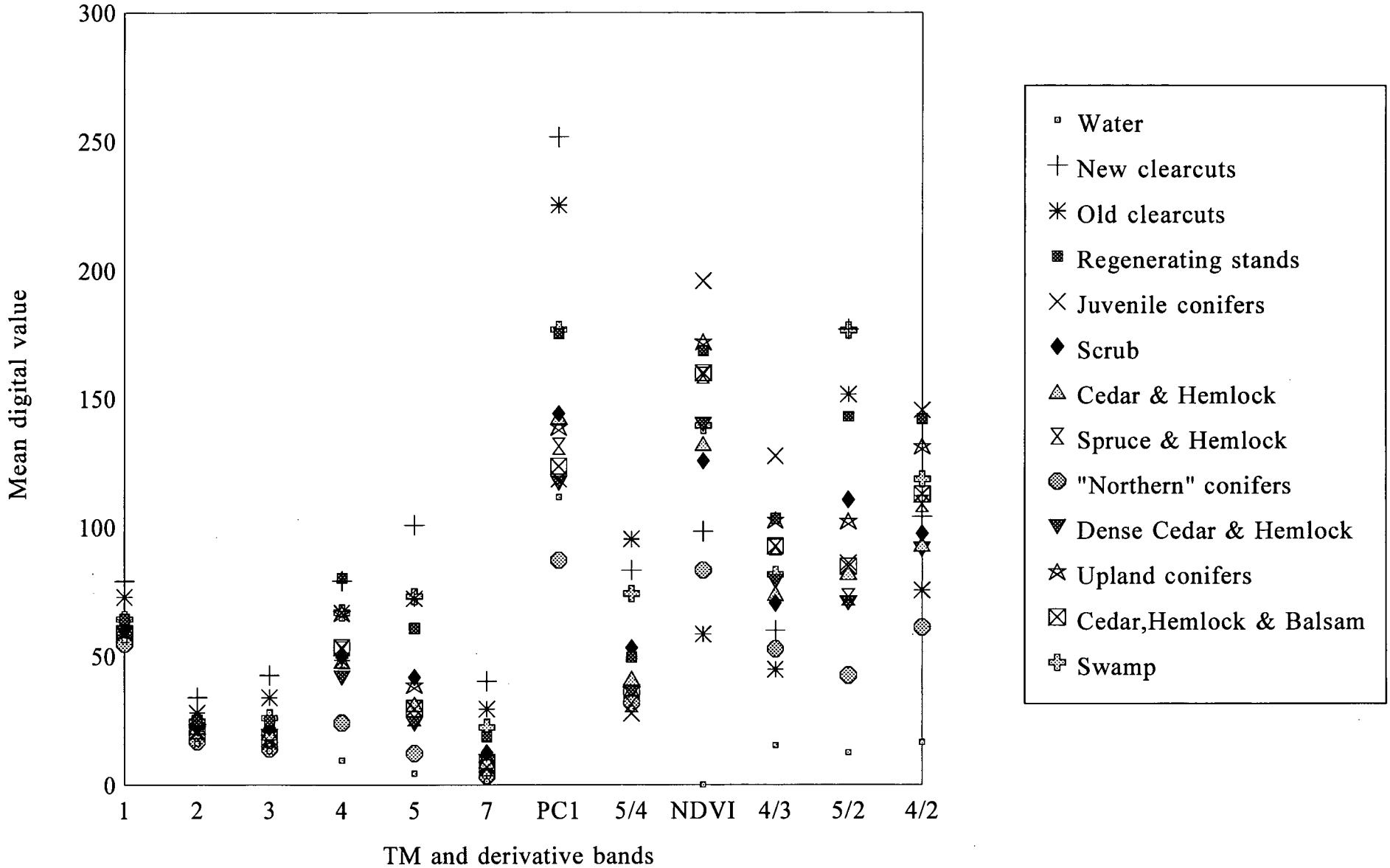

Figure 10b. September spectral pattern plots for cover type classes.

Table 9a. June Classification Error Matrix

	Forest Cover Map Classes (Reference Data)														
Landsat TM Classes	ncc	occ	reg	juv	scr	ch	sh	nc	dch	alp	uc	chf	wat	swa	**%Corr. (User's)**
ncc	**481**	38	4	0	6	22				3	46		18	1	**77.71**
occ	23	**1603**	31	2	101	61				12	124	8	46		**79.71**
reg	7	27	**738**	158	27	16	12			18	54	10		2	**69.17**
juv			66	**1007**	3	6	67		2	138	14	13	1		**76.46**
scr	2		1		**791**	156			17	1	119	8	3		**71.98**
ch				8	66	**2258**	5	44	25	3	20	107			**89.04**
sh			3	34	10	11	**499**	74	171	33	8	98			**53.03**
nc						7	27	**1149**	350			66	138		**66.15**
dch					4	16	139	272	**1696**	1		115			**75.61**
alp			16	205			25		1	**406**	161	12			**49.15**
uc			6	23	21	23	5		54	71	**1749**	58			**87.02**
chf			1	8	3	257	39	118	203	7	69	**661**			**48.39**
wat													**5367**		**100**
swa		10	12			1							75	**183**	**65.13**
% Corr.	**93.76**	**95.53**	**84.05**	**69.69**	**76.65**	**76.68**	**61.00**	**69.34**	**67.33**	**58.59**	**73.98**	**56.69**	**95.02**	**98.36**	

Table 9b. September Classification Error Matrix

	Forest Cover Map Classes (Reference Data)														
Landsat TM Classes	ncc	occ	reg	juv	scr	ch	sh	nc	dch	alp	uc	chf	wat	swa	**%Corr. (User's)**
ncc	**608**	98	9				1							1	**84.80**
occ	15	**1086**	10		25	1							19	2	**93.78**
reg	3	44	**453**	4	17					2	75			24	**72.83**
juv		20	21	**987**		12	22		2	175	60	10			**75.40**
scr	6		7	1	**803**	119			5		23	1	8		**82.53**
ch					34	**2813**	23	6	147		7	13			**92.44**
sh				32		53	**572**	20	90	11	7	42			**69.17**
nc								**2105**	6						**99.72**
dch					2	51	82	77	**1362**			51			**83.82**
alp				372			5	68	1	**619**	8	15			**56.89**
uc			11	40	4	37	15	51		11	**2083**	28			**91.36**
chf				8	2	47	43	14	104	9	263	**441**			**47.37**
wat								7					**6494**		**99.89**
swa	4	2	3										135	**154**	**51.68**
% Corr.	**95.60**	**86.88**	**88.13**	**68.35**	**90.53**	**89.79**	**74.97**	**86.05**	**79.32**	**74.85**	**82.46**	**73.38**	**79.41**	**85.08**	

Table 9c. Multitemporal Classification Error Matrix

	Forest Cover Map Classes (Reference Data)														
Landsat TM Classes	ncc	occ	reg	juv	scr	ch	sh	nc	dch	alp	uc	chf	wat	swa	**%Corr. (User's)**
ncc	**606**	85	7		2						14		32		**81.23**
occ	20	**1132**	9		4										**97.17**
reg	8	19	**485**	38	2		2				9			3	**85.69**
juv		1	1	**1335**			5		1	26	6	2			**96.95**
scr	2	13	6		**856**	69			1		3				**90.11**
ch					16	**2955**	10	207	177	2		13			**87.43**
sh				5		21	**679**	173	128	11		10			**66.12**
nc								**2071**	118				77		**91.40**
dch						56	37		**1795**	1		9			**94.57**
alp				57	6		8	7	4	**772**	19	12			**87.23**
uc				8		20	3	72	2	11	**2349**	26			**94.30**
chf				1	1	14	19	101	47	4	126	**529**			**62.83**
wat													**4271**		**100**
swa			6										176	**178**	**49.44**
% Corr.	**95.28**	**90.56**	**94.36**	**92.45**	**96.51**	**94.25**	**88.99**	**78.72**	**78.97**	**93.35**	**92.99**	**88.02**	**93.74**	**98.34**	

Key: Occ - old clear-cuts; ncc - new/recent clear-cuts; reg - regeneration stand; juv - juvenile stand; scr - scrub land; ch - cedar and hemlock stand of normal stocking; sh - sitka spruce and hemlock stand; nc - conifers on north facing slopes ("northern conifers"); dch - dense cedar and hemlock stand; alp - alpine conifers; chf - mixed cedar, hemlock, and fir; wat - water bodies; swa - swamp.

Figure 11. Results of maximum-likelihood classification of Carmanah TM data. Blue is water, light blue is clouds, cyan is shoreline, green is mixed cedar/hemlock stands of normal stocking, purple is upland conifers, red is mixed spruce and hemlock, orange is conifers on north-facing slopes, deep pink is new and old regenerating stands, light pink is alpine conifers, orange-yellow is densely stocked cedar and hemlock stands, yellow is cedar/hemlock/fir, violet is scrub stand, light violet is new clearcuts, pale violet is old clearcuts, light cyan is creeks, black is null class. (a) June, 1992 thematic map (b) September, 1992 thematic map (c) multitemporal (combined) thematic map.

(a)

(b)

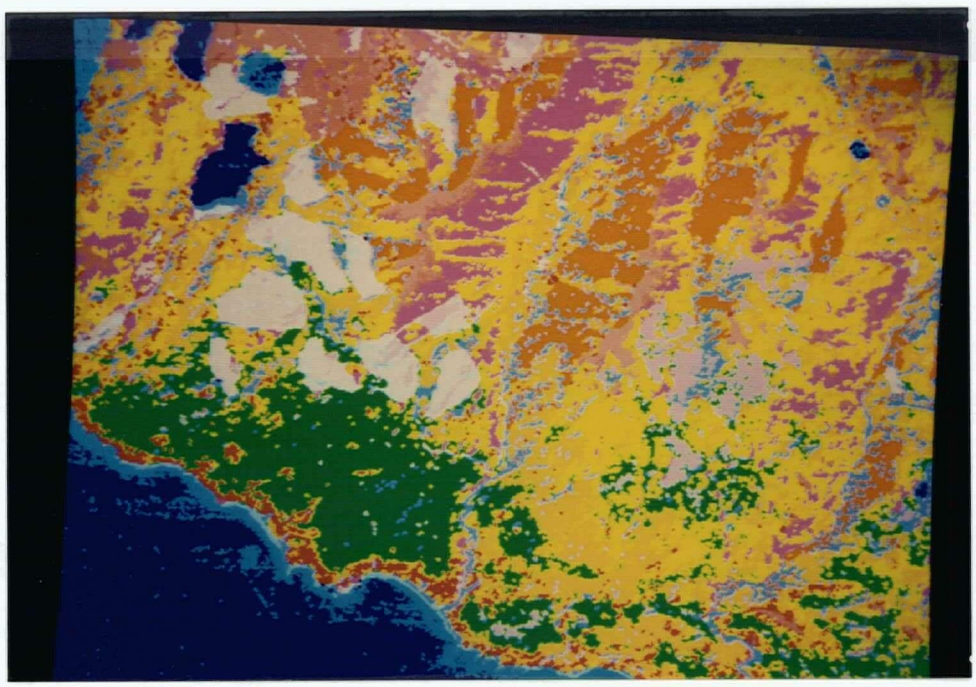

c)

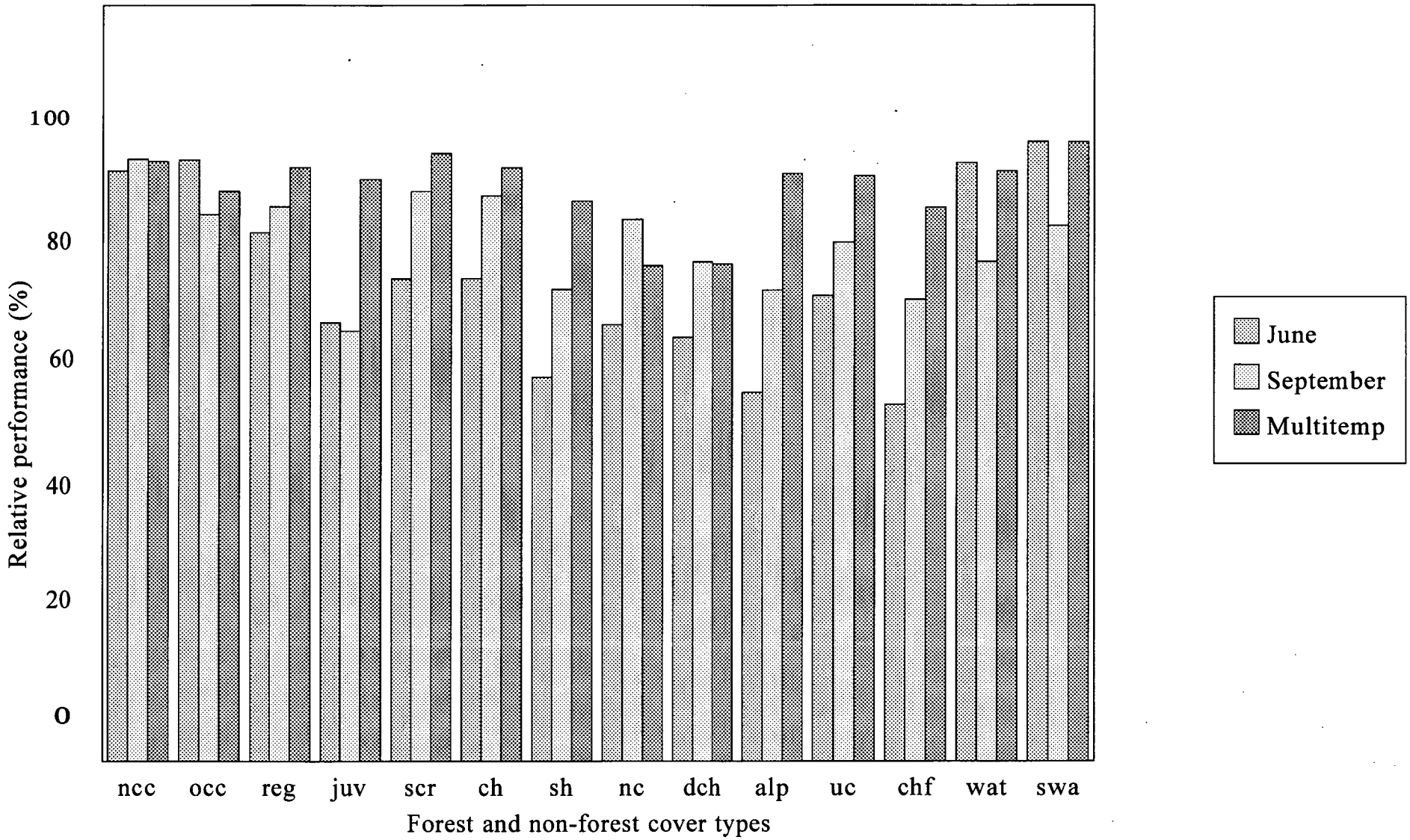

Figure 12. Comparison of classification of forest and non-forest classes.
(The definition for X-labels are given in page 54).

classification were significantly different from each other in classifying general cover types. The multitemporal classification of forest cover types was significantly different from the single date classifications. Between date comparison indicated that the September classification of forest cover types was significantly better than the June classification.

4.7 Change Detection

Image differencing, image ratioing and normalized difference vegetation index (NDVI) techniques were utilized to derive new images for each TM band. To minimize sensor calibration effects and standardize data acquisition, an atmospheric correction routine was applied. Atmospheric normalization was achieved through linear regression over time. Jensen (1983) reported that regression techniques account for differences in the mean and variance between pixel values for different dates so that adverse effects from the differences in atmospheric conditions or sun angles are reduced. The regression analysis was conducted on digital values from the entire TM dataset. SAS output for regressing the September data versus the June data are summarized in Table 11. All models were significant at $\alpha = 0.05$. A general trend seen in the table was an increase in R^2 from band 1 to band 5. With the exception of TM4 and TM5, SE_E decreased across the electromagnetic spectrum. However, relatively poor fits were obtained with TM bands 1 (blue) and 2 (green), although standard errors of the estimate (SE_E) were low. This indicates that the June DN values could not be relied upon for predicting the September digital values in the two spectral regions. As such, analysis was restricted to bands 3, 4, 5 and 7. Boundaries between change and no-change pixels were estimated using a statistical approach developed by Ingram *et al.* (1981) and recommended in many other studies. From visual analysis and histogram evaluation image, it can be seen that differences for bands 3 and 5 best indicated

Table 10a. [1]Scheffe's test for general cover type classification accuracies

Scheffe Grouping*		Mean Classification Accuracy	TM dataset
	A	91.181	Multitemporal
B	A	82.486	September
B		76.905	June

* Means with the same letter are not significantly different.
$\alpha = 0.05$
Critical difference (CD) = 9.6266

Table 10b. Scheffe's test for forest cover type classification accuracies

Scheffe Grouping*	Mean Classification Accuracy	TM dataset
A	89.122	Multitemporal
B	79.700	September
C	68.594	June

* Means with the same letter are not significantly different.
$\alpha = 0.05$
Critical difference (CD) = 9.3315

[1]Scheffe's procedure tests for pairwise differences in population means, u_i - u_j. The critical difference (CD) is computed as follows

$$CD = \sqrt{((k-1)F_{\alpha}(df1, df2))}\sqrt{(MSW(1/n_i + 1/n_j))}$$

where MSW represents the mean square difference within-groups-variance estimate, n_i and n_j are the sizes of the ith and jth samples respectively and k is the number of treatments or means to be compared. There is a significant difference between the two means being compared when the difference between their means is greater than CD.

the changes that occurred between June and September. The thresholding image to bitmap (THR) algorithm provided by PCI was used to density slice the new images in order to display suspected changes.

Generally, minor to no changes were observed for most forest cover types in the differenced and ratioed images. This was not surprising given the short time interval and abolition of clear-cutting and other forest disturbances in Carmanah Valley. However, noted changes in radiance (tonal difference) were suspected to be related to high reflectance expected during early summer. This was highlighted for clearcuts which appeared in bright tones in both derivative images. Cloud cover stood out as a major non-forest change between the two dates. NDVI analysis produced similar results. The difference between the June and the September NDVI resulted in small (zero in most cases) digital values. This indicated that no significant change occurred with respect to forest biomass or forest canopy.

4.8 Comparative Analysis of Classified Data

Classified images were assessed for their capability to show likely trends and discriminate groups that are of interest in forest management. Comparative analysis involved looking at species composition, age classes and stocking level among other forest parameters. As illustrated earlier and shown in Figures 13a and 13b, the June digital values were generally higher than those from September. A general spectral pattern of moderately low mean DN in the red band followed by a relatively high mean near-infrared digital value and low to moderate mean DN in the mid-infrared spectral region was observed for both dates. Enhanced image ratios magnified the change in digital values across the electromagnetic spectrum. For example, the high TM4/3 ratio of alpine conifers for both dates indicated higher near-infrared digital numbers compared to the red band. High PC1 (visible)

Table 11. Regression Analysis Results

Fitted linear regression model	R^2	SE_E
B91 = 11.22 + 0.54B61	0.25	4.81
B92 = -0.39 + 0.6B62	0.36	2.74
B93 = -2.82 + 0.61B63	0.75	2.63
B94 = -14.48 + 0.91B64	0.85	7.52
B95 = -14.57 + 0.91B65	0.86	5.62
B97 = -5.81 + 0.85B67	0.81	2.47

Table 12. Classification accuracies for age and stocking classes

	Classification Accuracy	
Age classes	June, '92 TM data	September, '92 TM data
Juvenile (>20 yrs)	85.84	87.94
Immature (21-100 yrs)	77.55	67.87
Mature (100+ yrs)	76.26	85.54
Stocking levels		
Non-stocked	94.65	90.88
Low stocked	77.29	70.05
Medium stocked	70.9	84.34
Highly stocked	50.51	74.12

values for upland conifers (June) and alpine conifers (September) were expected given they were located on south-facing slopes. At the lowest end of PC1 were mixed cedar and hemlock stands in June and conifers on north-facing slopes in September. On both occasions, alpine conifers and conifers on north-facing slopes had the highest and lowest mean NDVI values respectively. With the exception of mixed spruce and hemlock stands, all other forest cover types showed almost similar mean NDVI values in June. On the other hand, the NDVI values in September scene provided a wide separation between forest types.

Comparison of classification accuracies (Figure 12) indicated that a better classification was achieved with the September image than with the June image. This observation supports the wide spectral separation offered by September scene (Figure 13b). TM bands 3, 4 and 5 provided a narrow spectral separabilty. The high classification accuracy's achieved was thus due to discrimination provided by derivative bands.

As detailed age information on a stand by stand basis was not available, general age groupings as given by forest cover maps were adopted. These included juvenile (less than 20 years old), maturing (between 21 and 100 years old) and mature or oldgrowth (greater than 100 years). Figures 14a and 14b presents their spectral pattern plots. Juvenile stands had higher mean DN values than either maturing or mature stands in the visible, near-infrared and mid-infrared spectral regions. Mature stands had the lowest mean digital values in all three spectral regions. Juvenile and maturing stands registered the highest NDVI values in the June and September scenes respectively. Lowest NDVI and PC1 and 4/3 values recorded for mature/oldgrowth stands in June. Classification of mixed cedar and hemlock stands into their respective age categories is summarized in Table 12 (see page 61). On average all three age classes were accurately classified in both images. However, mature stands were classified

more poorly in the June image than in the September image. This was surprising given the wide spectral separation provided by near-infrared and derivative bands. In the September scene, immature stands had mean DN values close to those of juvenile stands in the red and near-infrared bands and close to those of mature stands in the red and mid-infrared spectral regions. As a result, the classifiers could not make a complete discrimination of this age class from either juvenile or mature stands. This may explain the observed low classification accuracy (67.87%) of immature stands in the September image compared to that achieved with the June image. Oldgrowth/mature forest was better classified (85.54) by the September image.

Four stocking levels were considered: non-stocked, low, medium and high. Non-stocked stands included new and old clearcuts. Spectral patterns for stocking classes are presented in Figures 15a and 15b. Medium stocked conifers had the highest near-infrared and mid-infrared mean DNs and highly stocked conifers showed the lowest mean digital values for all three TM bands. The latter observation appears to be as a result of the small size of selected sites. TM bands 4 and 5 provided a good separation of stocking levels. As for derivative bands, medium stocked stands had the highest PC1 and NDVI values. In the September image, non-stocked and low stocked stands had similar PC1 values, and low stocked and high stocked stands had similar NDVI values. A summary of classification accuracies of mixed cedar and hemlock stocking levels are given in Table 12 (see page 61). Both images discriminated non-stocked stands with a better accuracy than the other stocking classes, 94.65 percent and 90.88 percent in the June and September images respectively. This was not surprising given non-stocked stands unique spectral pattern. The September image provided a better classification for medium and high stocked stands. A better delineation of low stocked stands was achieved with the June image. The exceptionally poor June classification for highly stocked stands was at first surprising

given the unique spectral pattern of this class. However, a close examination of this type revealed that cloud cover was most dominant over its vicinity.

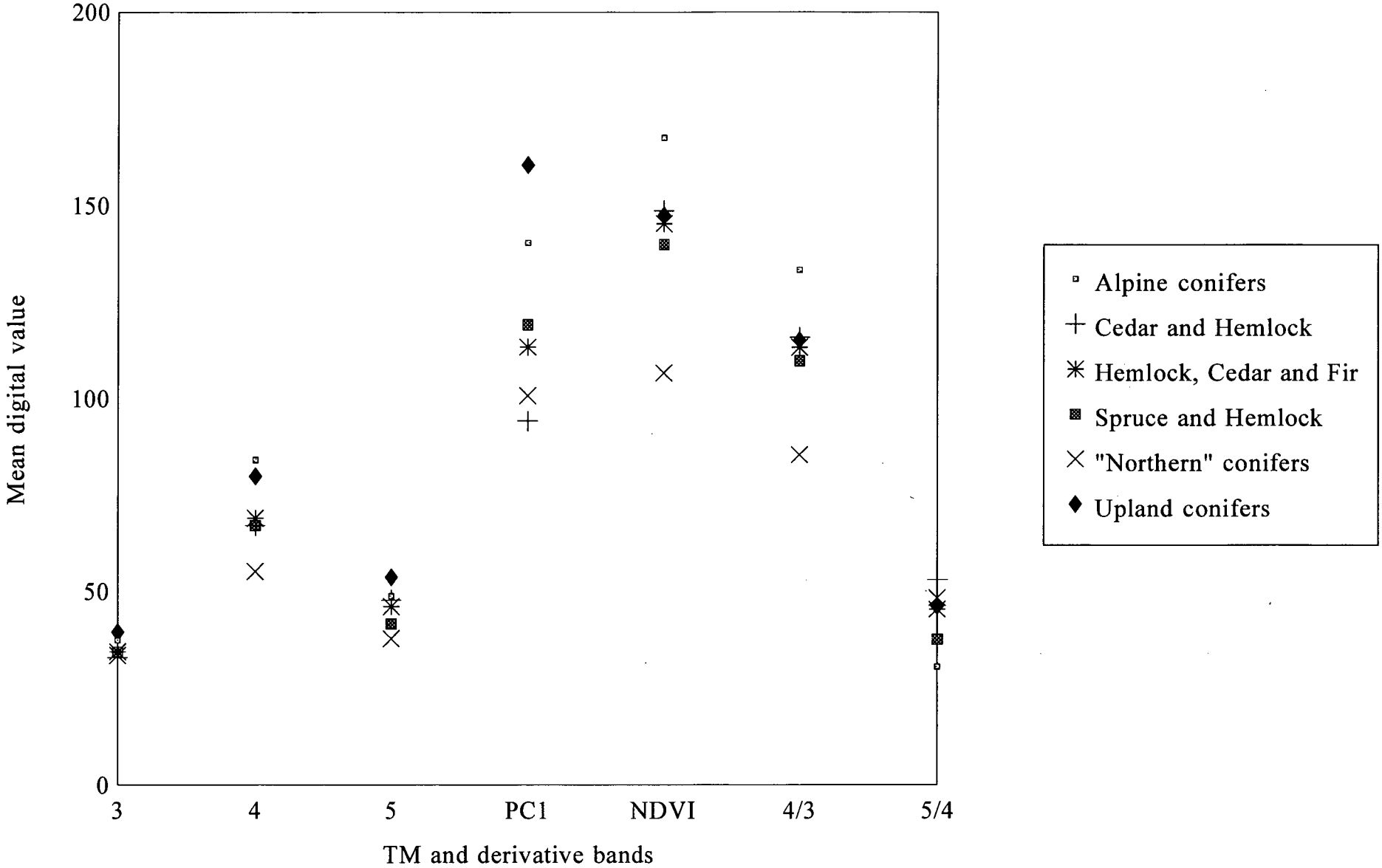

Figure 13a. Spectral pattern plots for forest cover types in June image.

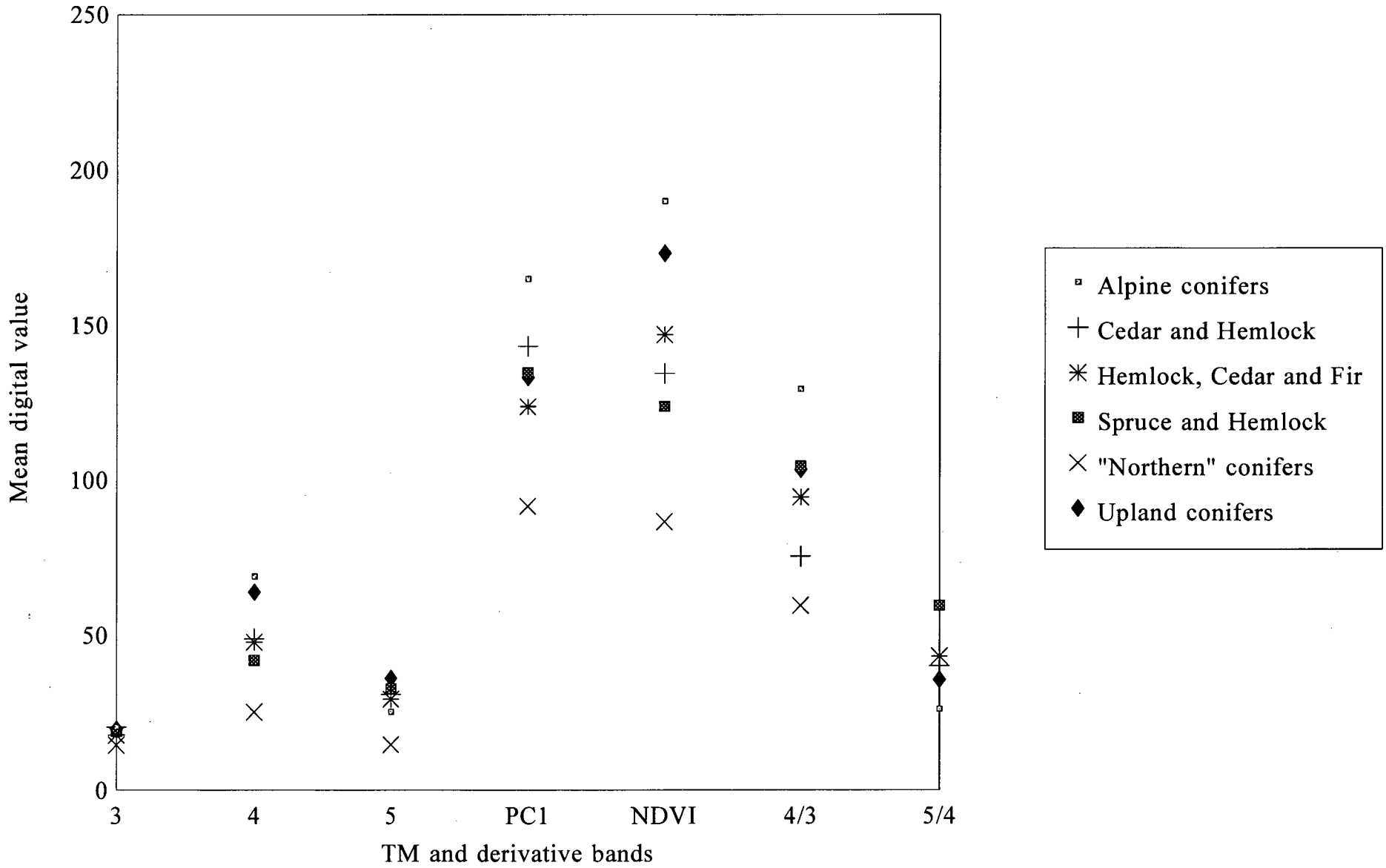

Figure 13b. Spectral pattern plots for forest cover types in September image.

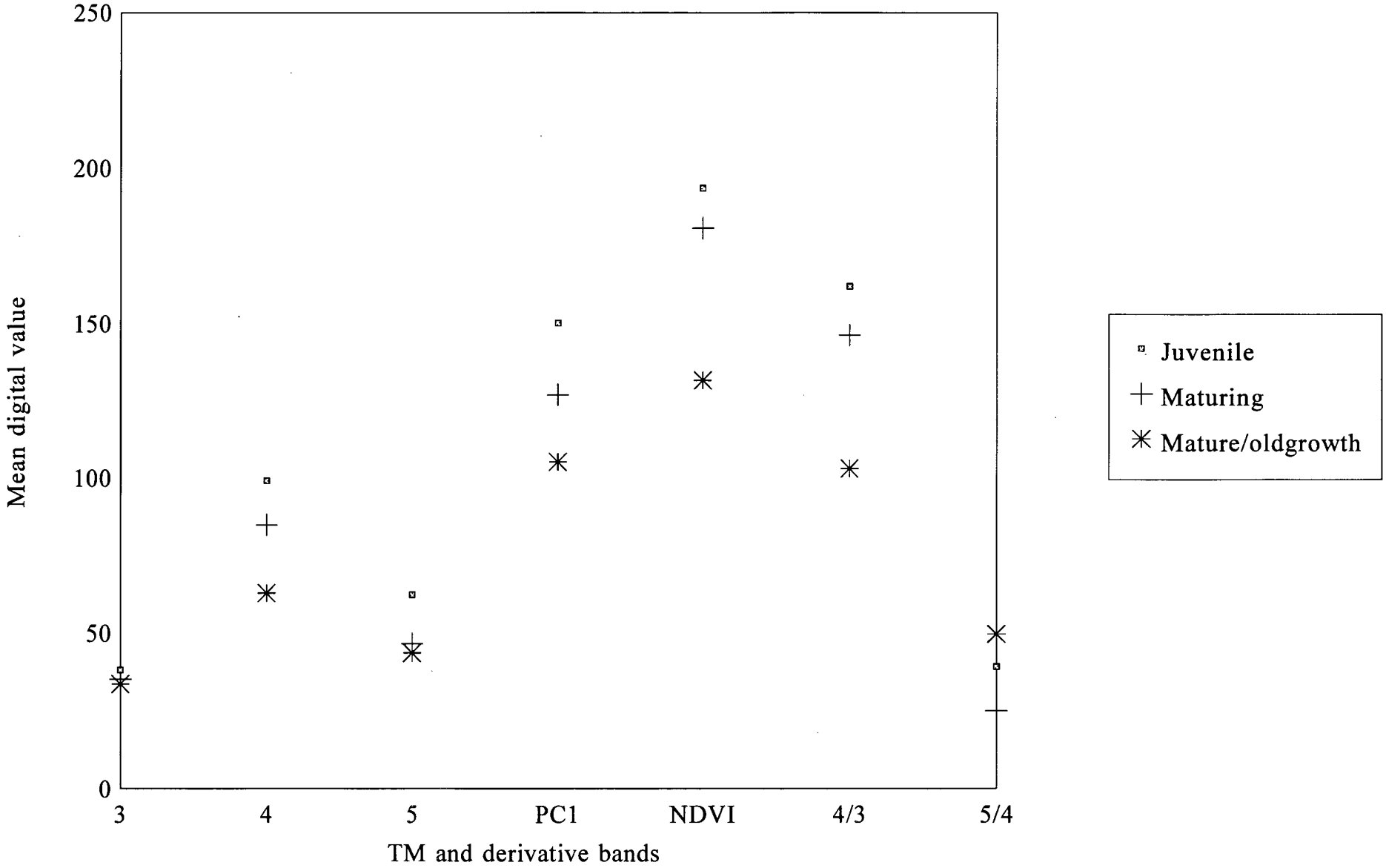

Figure 14a. Spectral pattern plots for forest age classes in June image.

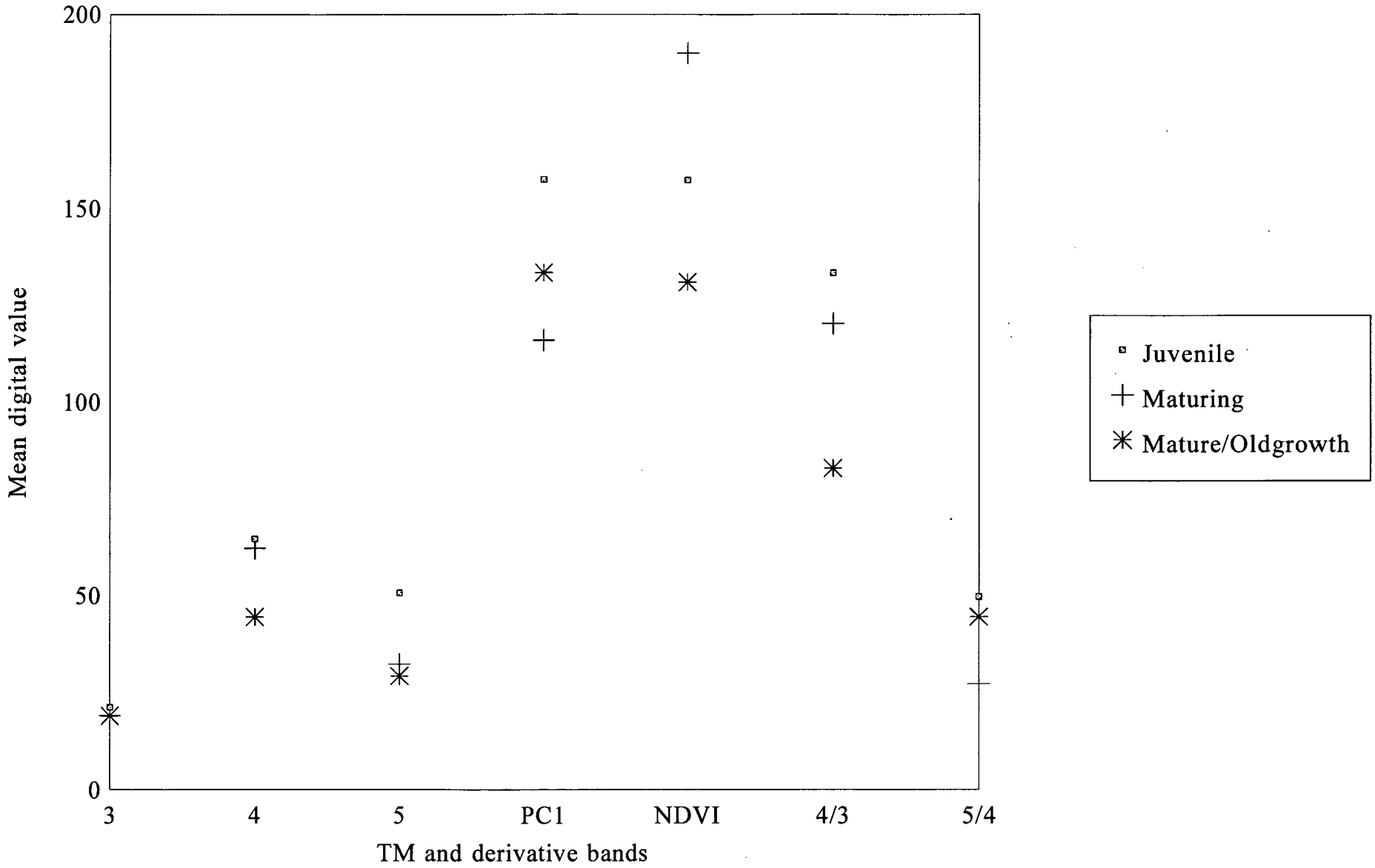

Figure 14b. Spectral pattern plots for forest age classes in September image.

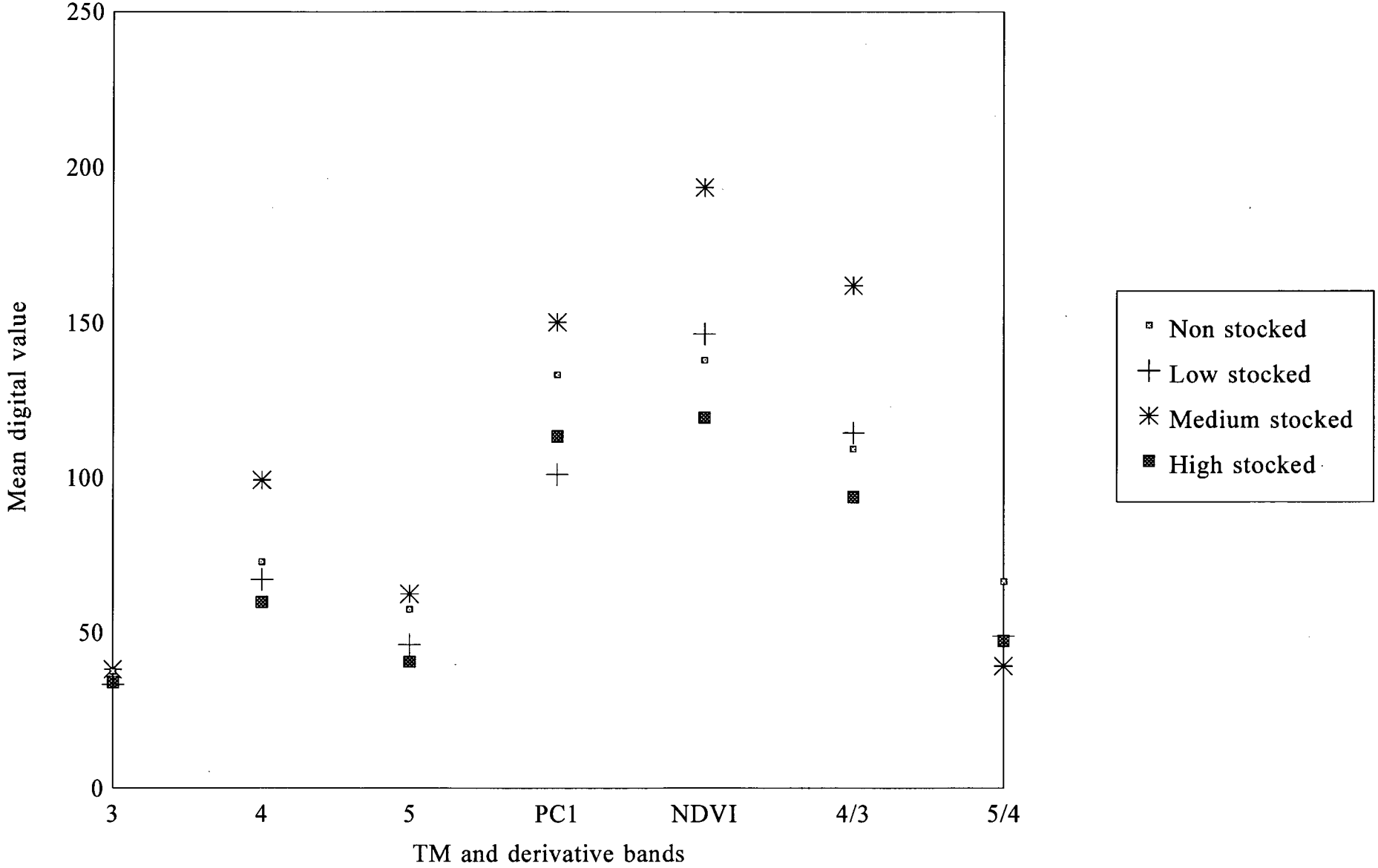

Figure 15a. Spectal pattern plots for stocking classes in June image.

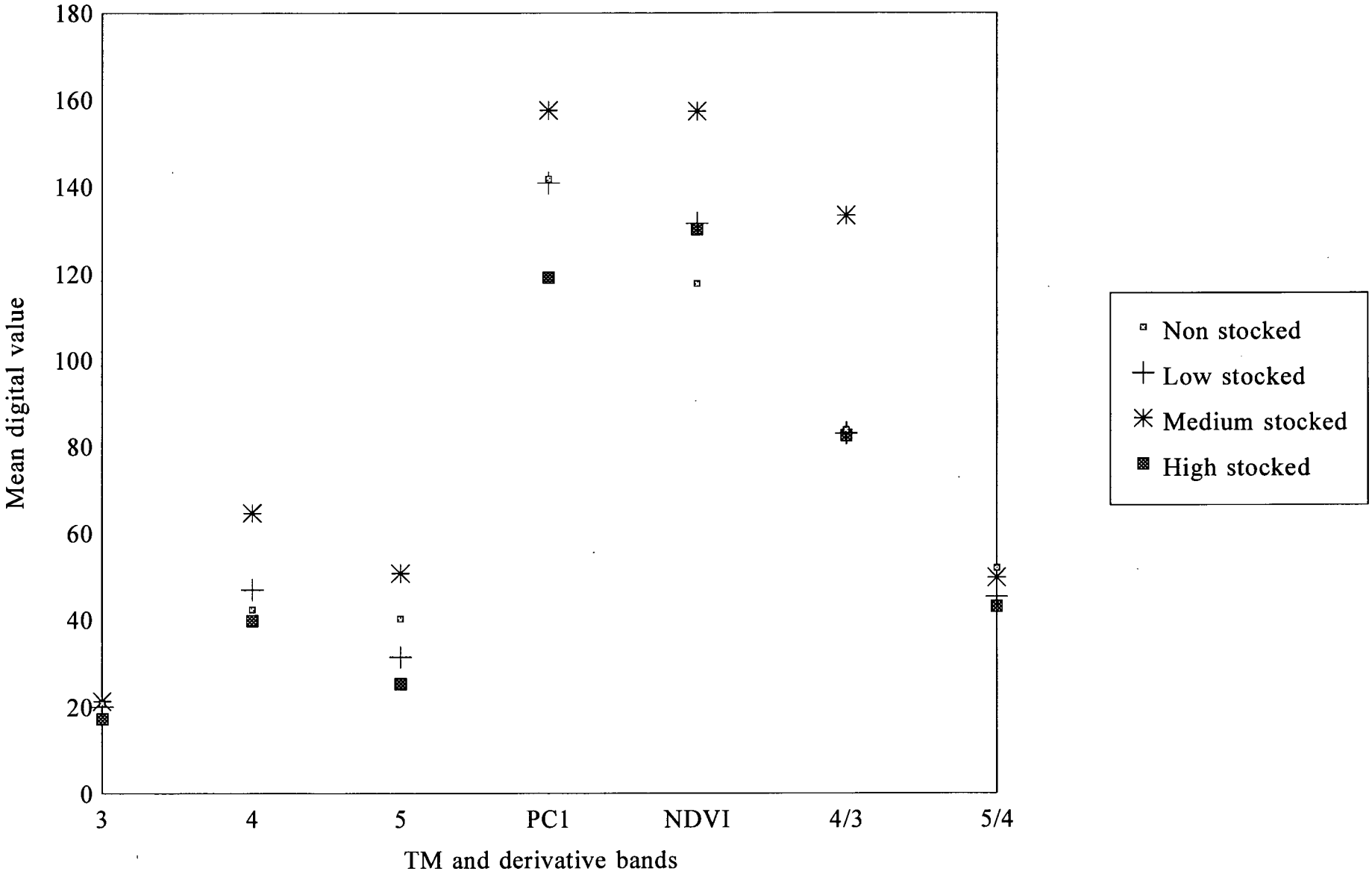

Figure 15b. Spectral pattern plots for stocking classes in September image.

4.9 Discussion

The primary interest of this study was to test for temporal discrimination of the forest cover types in Carmanah Valley using the June and September TM data. A first step towards this objective involved determining the information content of TM dataset and ways of handling this data more efficiently. A principal component analysis (PCA) approach was adopted in an attempt to enhance TM images for visual interpretation (i.e., to select the best bands and features for display). Additionally, the PCA approach aided in understanding the fundamental spectral feature space and dimensionality of the TM data.

Two forms of PCA were carried out, namely "standard PCA" and "selective PCA". In the former, all reflective TM bands were used as input, whereas in the latter only a subset of TM bands were used as input. Attention is first given to "standard PCA". A large portion of information for both dates was compressed to the first three principal components, specifically 97.63 percent in the June and 97.6 percent in the September images. In a statistical sense, a vast amount of information about general cover types of the Carmanah valley can thus be presented in a three-feature subset of the TM data. This result is in agreement with the observations of Townshend *et al.* (1983) and Crist and Cicone (1984) that TM data occupies three spectral dimensions.

All six TM bands contributed to the variation seen in the first three principal components. Their contribution, as shown by the eigenvectors, varied from one component to another. Striking similarities could be seen between the PCA runs on the June and the September images. TM bands 2, 3, 5 and 7 loaded strongly to the first principal component (PC1) with TM bands 1 and 4 loading strongly to the second principal component (PC2). TM bands 4 and 7 loaded strongly to the third component (PC3). PC1 was thus a sum of visible and mid-infrared regions. Visually it appeared in

brighter tones (Figures 5a and 6a - see pages 36 and 37). Clearcuts, water bodies and swamps were highly emphasized. Except for scrub land, the majority of the forest cover types were difficult to discriminate. PC2, as mentioned, was a blue-green to near infrared contrast. A substantial amount of spectral contrast was evident in this feature (Figures 5b and 6b). The appearance of clearcuts in dark tones contrasted sharply to its bright tones in PC1. This reflects the fact that principal components are orthogonal to each other. PC2 highlighted some of the cover types that were obscured by the more dominant features in PC1. Among these were logging roads, rivers/creeks, south-facing slopes, scrubland, regeneration stands (bright toned) and a wide range of other forest cover types. An interesting observation was the complete absence of shadows on the north-facing slopes (illumination of shadowed areas). This allowed for evaluation of the minimal reflectance from "shadowed" slopes. PC3 appeared to be a contrast between near-infrared and mid-infrared. As shown in Figures 5c and 6c (pages 37 and 38), PC3 highlighted logging roads within cutblocks (i.e., bright pixels on a dark background). Its tonal reversal in PC3 compared to PC2 again illustrates the lack of correlation between the two images and the significant amount of noise present in PC3. A disadvantage of PC3 was it's sensitivity to cloud cover in June. Hardly any meaningful discrimination could be made across a large portion of the June PC3 image. Thus only PC1 and PC2 were useful for forest cover typing in this scene. The fourth, fifth and sixth principal component contained lots of noise, and thus they were not useful for either image generation or information extraction.

In selective PCA, TM bands were first grouped into their respective spectral regions. Separate PCA was conducted on the visible and mid-infrared group in an attempt to select a representative band in each region. The object was to generate bands for colour compositing to be used in visual analysis. Band selection was achieved with the aid of eigenvectors loadings of each chosen principal component.

In both the June and September images, band 3 was selected from the visible region and band 5 was chosen from the mid-infrared region. As a result, a representative colour composite for visual analysis was derived by loading band 4 in the red gun, band 5 in the green gun and band 3 in the blue band. This derivation is in agreement with many research results and authors including Horler and Ahern (1986) that TM bands 3, 4 and 5 perform almost as well as the first three principal components for ground cover type discrimination.

An additional optimum colour composite was generated using selective PCA results. PC1 of the visible region was loaded to the blue gun, band 4 to the green gun and PC1 of the mid-infrared to the red gun. As presented in Tables 5a and 5b (see page 40), PC1 in each spectral region explained a vast amount of image information (i.e., 87.38 percent (June) and 91.56 percent (September) in the visible region, and 96.81 percent (June) and 96.94 percent (September) in the mid-infrared region). Using selective PCA in this manner allowed for dimensional reduction with little loss of information. The components not used contained minimal left over variation. A number of enhancements (IHS) were performed on the composite to achieve the image shown in Figures 7a and 7b (see page 42). This composite looked similar to a normal colour composite made from three original TM bands and was found to be easier to interpret. Forest and other cover types appeared in distinct colours and were in fact categorized like in a thematic map. It is here that possible training areas were detected and identified, and their locations taken into account. Among other features, two classes of clearcuts were clearly evident in both the June and September images. Other visible cover types included alpine conifers, mixed conifers (mainly cedar and hemlock stands) and cedar and spruce stands, scrub land, regenerations, swamps and upland conifers or sunlit conifers.

The purpose of the second run of selective PCA was to look at the spectral contrast in the multitemporal TM data. Specifically, to identify the new information contributed by each band that is not contained in the others. It was hypothesized from the outset that mapping information unique to each band could be the key to discrimination of forest cover types of the Carmanah Valley. Combined June and September TM data was used in this run. Band correlations between dates were first evaluated. Low correlation was observed between visible and near-infrared, visible and mid-infrared, and near-infrared and mid-infrared. Pairs of less correlated bands were input into a PCA. In an attempt to map possible spectral contrasts between all spectral regions and temporal contrast, a total of nine band pairs were used. In general, the degree of correlation between any two bands appeared to be related to the amount of spectral and temporal contrast. Information common or similar to both bands was mapped to the first principal component and information unique to either of the bands was mapped to the second principal component. The higher the correlation, the more similar were the bands and the less the spectral contrast (more common information in the first principal component). The lower the band correlation, the more the spectral contrast (Table 8 - see page 44). PC2 of each image pair was interpreted one at a time in a black and white mode. The image derived from band pairs 61 and 94, 63 and 94, 64 and 91, and 64 and 92 highlighted the spectral contrast between forest cover types and other vegetation cover. Regeneration, stands of mixed conifers dominated by hemlock with varying proportions of spruce, cedar and fir, could be vaguely detected and the extent of scrub land was obvious (Figures 8a and 8b - see page 47). Tonal difference between oldgrowth and young or juvenile stands was emphasized with the former appearing in dark to moderate tones and the latter in brighter tones. Location and extent of these forest age classes were noted for later digital analysis. Alpine conifers, like regenerating stands, appeared in bright tones. Scrub land in September was highlighted,

appearing in dark tones, a sharp contrast to the surrounding forest cover types. Clearcuts at both dates took very dark tones. At this point, enhancements performed so far were deemed sufficient and attention was directed to digital classification.

There was a great temptation to load all available bands into a maximum-likelihood classifier (MLC). However, reduction of TM data has been demonstrated to significantly improve the processing efficiency of a classifier (Horler and Ahern, 1986). Towards this objective, TM bands 1, 2, 3, 4, 5, and 7, and six derivative bands namely principal components (visible and shortwave-infrared bands), NDVI and image ratios 4/3, 5/4 and 5/2 were subjected to spectral pattern analysis for selection of band combinations most useful for cover-type discrimination. In both the June and September images, TM bands 3, 4 and 5 were chosen. PC1 (visible region), NDVI and image ratios 4/3 and 5/4 were also included in the optimal subset. However utilization of six bands out of a possible twelve bands was not considered a major TM band reduction. In effect, classification efficiency was sacrificed at the expense of accurate discrimination of cover types.

Paradoxically, classification accuracy appeared to be related to interband correlation. With low interband correlation, classification accuracy improved significantly over that found with high interband correlation. This was demonstrated by a poorly correlated subset of six bands (original and derivative bands) as opposed to twelve bands with some highly correlated. As evident from the correlation matrix (Tables 3a and 3b - see page 34), there was a relatively low interband correlation between TM bands 3, 4 and 5 on both occasions. A possible cause for this correlation stems from the combined influence of vegetated and non-vegetated surfaces absorbing red radiation (TM3), plant canopy structure and other surface properties reflecting near-infrared radiation (TM4) and plant canopy moisture and other moist surface properties absorbing short-wave infrared radiation (DeGloria, 1983).

Classification of forest cover types of Carmanah valley turned out to be a difficult task. The majority of forest stands appeared in mixtures of two or more species which differed in size, stocking, crown closure and age. This extreme forest complexity and narrow cover types for spectral "seperability" complicated identification of forest types at a species level. Numerous forest cover classes were documented by forest cover maps. It was apparent that such a detailed classification was not possible with the TM data. Reference data were condensed into 18 and 17 cover types (12 forest and 6/5 non-forest classes) for the June and September images respectively. Ironically, more spectral classes were generated by the unsupervised approach than were being explained by the supervised approach. Unfortunately, most of the spectral clusters possible with the unsupervised approach were difficult to identify and define.

The intent of the study was not to maximize classification accuracy. Instead, interest was centred on providing a method for comparing three separate classifications of forest cover types and other forest parameters. Variability of spectral characteristics of forest cover types was maximized during multitemporal classification. Classification results showed that multitemporal classification were more accurate than single-stage classification. The multidate approach to classification of forest cover types yielded an average classification accuracy approximately 20.5 percent and 9.4 percent greater than that of the June and September image, respectively. Additionally, mean classification accuracy of the multitemporal data was significantly better than that of either of the single-dates. It is expected that even better improvements in classification performance than those achieved may be possible through merger of multidate data that is properly timed (that is, to avoid cloud cover and restrict data acquisition to the best season of the year). However, with respect to general cover types, there was no significant difference between the multitemporal classification and the September classification. This

suggests that single date dataset performed as well as multitemporal dataset in classifying non-forest cover types.

Differing solar angles and uneven illumination conditions are expected between early- summer and late-summer. As a result, reflectance for any given cover type varied extensively between June and September. Spectral complexity that arose from a myriad of spectral signatures for each class was reduced to a great extent by moderate to high band correlation between dates. However, primary discriminatory power comes from low interband correlation between dates (e.g. band 64 versus band 97). In totality, the combination of seasonal variability and low interband correlation was responsible for the clean, sharp and accurate thematic map shown in Figure 11c (see page 56). An 'accurate' delineation of cover type extent was achieved. Cloud cover classified over ocean waters was a class attributed to June scene. This illustrates how seasonal variability was taken into account in the multitemporal data set. Improved classification was not without exception. Old clearcuts and north facing slope conifers were better classified in the June and September images, respectively. Moisture conditions and shadowing effect were suspected to have influenced discrimination of these cover types.

Classification accuracy of the majority of cover-types was generally higher in September than in June. The mean September classification accuracy of forest-cover types was shown to be significantly better than June's. This was an interesting observation. It was originally hypothesized that with the sun being at it's zenith in June, higher reflectance is expected in early summer. The improved performance of the September data was attributed to cloud cover in June, whose influence was more pronounced in the visible region. June spectral reflectance was suspected to be coming from both ground features and clouds. Uneven distribution of cloud cover over the entire scene further complicated spectral variability. For instance, at one point a given cover type, (e.g. mixed cedar and

hemlock stands) was covered by clouds but cloud-free at another point. Consequently, the MLC classifier ended up identifying two spectral classes from the same information class. Unfortunately, the cloud cover component could not be removed or accounted for in digital analysis. Another possible cause is that unique reflectance characteristics of cover types may have been more enhanced (hence more spectral information) in the September scene. Indeed, TM bands 4 and 5 in the September image (Figure 13b) provided a slightly wider spectral separation between forest types. This is in agreement with Walsh's (1980) observation that September imagery provided more information than early summer MSS data due to the phenological condition of vegetation and the lower sun angle. However, September superiority was not without exception, especially where there was no or minimal cloud cover in the June image. Old clearcuts and juvenile conifers were better classified by the June image by a margin of 8.6 percent and 1.4 percent, respectively. It should be mentioned here that both the June and September data discriminated the same forest cover types. Other than improving classification accuracies, seasonal variability hardly aided in delineating additional forest cover types.

A characteristic spectral pattern of low red, high near-infrared, and moderate mid-infrared mean DN values, was shown for all forest cover types in both the June and September images. On the one hand, this observation indicated that a significant amount of spectral reflectance could be attributed to forest cover types and that there was a similar spectral variation among forest cover types despite cloud cover in June. This narrow spectral variability was attributed to the fact that coniferous trees were the only species cover types under consideration. Other possible causes include complex coniferous mixtures and hemlock dominance in all mixed stands. Some initial training sets showed no promise in separating certain classes (e.g., mixed hemlock/cedar stands versus mixed hemlock/cedar/spruce stands). These two stands were among cover types that accounted for most of

the off-diagonal errors. This made sense because there are so many factors which affect spectral reflectance of mixed types. On the other hand, it was extremely difficult to identify individual trees with unique and pronounced features. A case in point involved the reputed tall(est) sitka spruces. While this group of trees appear in sharp contrast on the ground, TM data could hardly separate them from the rest of the forest.

Current information on the location and distribution of all ages and structures is needed to manage public lands for multiple use objectives. Information on younger stand development is necessary and critical in determining future timber supply and wildlife habitat (Harris, 1984). Furthermore, the identification of the remaining stands of oldgrowth forest has been recently highlighted (Ripple *et al.*, 1991). In a study of age classes, juvenile stands were seen to have higher mean digital values than either immature or mature/oldgrowth forest stands. This was observed in both visual and infrared bands. The trend observed was that there was a decrease in mean digital values in the three spectral regions with an increase in stand age. This correlation may be due to the increased proportion of older foliage age-classes compared to current year foliage as the conifers matures. One other possible cause is that absorption of plant pigments (e.g., chlorophyll a and chlorophyll b) and moisture tend to increase with stand age (as suggested by Spanner *et al.*, (1989)).

This study suggests that general stocking classes can be discriminated by TM data. The September image, on average, provided better stocking class discrimination than the June image. Higher classification accuracies for non-stocked areas were expected given their unique spectral patterns. The order of mean digital values, from highest to lowest for stocking classes was as follows: medium stocked, low stocked and high stocked. This demonstrated poor or no correlation between mean digital values and stocking. The fact that highly stocked stands had the lowest digital values came

as a surprise. With this kind of stand, there are few if any gaps and shadowing is at a minimum. Additionally there is maximum reflectance. Possible causes could be the nature of canopy stratification and the structure of mixed coniferous stands or that insufficient training pixels were used for this class.

Chapter 5

Conclusions

Assessment of the six principal components generated from the reflective TM bands indicated that the first three principal components of the TM data explained a vast amount of image information. This suggests that the intrinsic dimensionality of the TM data was three.

Candidate bands used in selective PCA included visible and mid-infrared bands on the one hand and less correlated band pairs on the other hand. In this run of PCA, a dimensionally reduced and enhanced composite in the form of PC1 (visible), TM4 and PC1 (mid-infrared) was obtained. Major TM reflective spectral regions were represented in this composite (i.e., visible-TM 1, 2, or 3, near-infrared-TM 4 and mid-infrared-TM 5 or 7). This composite was a lot easier to visually interpret and was, as such, utilized in of the most visual analyses. An image analyst who relies heavily on visual analysis for information extraction may want to generate such a composite.

In mapping spectral contrasts between spectral regions, the degree of correlation between any two bands was observed to be related to the amount of spectral contrast. The higher the correlation, the less was the spectral contrast and the lower the correlation, the more was the spectral contrast. Less correlated TM bands 3, 4 and 5 provided the best discrimination among candidate forest cover types. These bands and their derivatives in the form of 4/3 and 5/4 and NDVI were included in the optimum band combination for maximum-likelihood classification. Before performing supervised

classification, it is crucial to determine the degree of interband correlation and to use only those bands that are poorly correlated to each other. This improves both classification efficiency and classification accuracy.

It may be too optimistic to conclude that forest cover types in the Carmanah Valley can be discriminated by TM data. The multitemporal approach to classification of forest cover types, combined with a specific knowledge of cover-type characteristics and attributes, is preferable to single-date classifications. Combining imagery helped to increase forest cover type classification accuracy. Indeed, classification involving multidate imagery resulted in classification accuracies greater than 90 percent for some cover types, and was significantly better than single-date classifications. It can be inferred that multi-date TM data may map specific forest cover types more effectively and accurately. Off-diagonal elements (misclassification) tended to be between related cover types. This was expected given that the majority of Carmanah forest stands are complex mixtures of two or more species which differ in size, density, crown closure, and age.

Based on classification performance achieved with TM bands 3, 4 and 5 in the combined multitemporal data set, it is suggested that would-be users of Landsat TM data in forest cover type mapping may need to limit data purchase to the three bands or at least a band from the visible, near-infrared and mid-infrared. Instead of ordering complete sets of multitemporal TM data, it could be cost effective to order multitemporal sets containing only the three bands. This reduces data cost and at the same time limits analysis to TM bands that contain a vast amount of spectral information. Atmospheric correction and geometric rectification should be mandatory, as this extra effort is worth the additional information and improved classification accuracy that results.

The classification results also indicated that time of the year can significantly affect cover-type classification accuracy. The classified forest cover types from the September image were significantly better than those from the June scene. The September TM data are thus a suitable dataset to recommend to users. It may be a suitable time to recommend for an overpass, but the superiority of this date may be solely because of cloud cover in June. In contrast, the June TM data appeared to contain high digital values than the September data. It is thus too early to generalize the conclusion, due to the observed atmospheric effects. Future studies should attempt to avoid cloud conditions. Only then can objective comparisons be made. In closing, it should be noted that both the June and September scenes looked similar in the "quicklook" imagery. Evidence of the cloud cover in the June scene was not apparent until image analysis began.

Classification accuracies achieved here were overly optimistic. Forest cover type maps were used as reference data and possibly could contain errors of omission and commission. Additionally, test areas covered training sites used in the classification process, thus they were not independent but large and evenly distributed. However, with a general forest cover type definition adopted in this study, "accurate classification" may be expected. Still, there is need to validate these accuracies.

The TM data under study appeared to contain information related to stand density, regeneration and age. Assessment of these forest parameters was achieved with spectral pattern analysis and maximum likelihood classifications. Non-stocked, low-stocked, medium stocked and high stocked stands were discriminated reasonably well. A trend was established between stand age and digital values. With an increase in stand age, there was a decrease in mean digital values in all TM bands considered.

The foregoing results were not without exception. The level of detailed forestry information possible from Landsat TM data was found to be limiting. Not only was it difficult to identify and map species, but also other forest parameters such as height class, dbh class, volume class, crown closure and canopy structure proved to be extremely difficult to detect. Statistics generated, through the unsupervised approach, contained more variables (spectral clusters) than were being explained by forest cover maps. A future study should therefore strive for detailed reference data that contain more information regarding specific Carmanah forest cover types.

Spectral reflectance appeared to be related to topography. Although sunlit and shadowed slopes were analysed separately, the effect of aspect was not satisfactorily accounted for. Since some spectral variance is topographically induced a future study should include topography in the form of slope, aspect, and elevation or use a digital elevation model (DEM). This may improve cover type discrimination.

In summary, given the choice of only one scene, the evidence seems to be in favour of the September imagery for assessment of the oldgrowth, temperate, coniferous rainforest.

Literature Cited

Aronoff, S., 1989. Geographic Information Systems: A Management Perspective. WDL Publications, Ottawa, Canada. 294pp.

Benson, A. S., and S. D. DeGloria, 1985. Interpretation of Landsat-4 Thematic Mapper and Multispectral Scanner Data for Forest Surveys, Photogrammetric Engineering and Remote Sensing, Vol. 51, No. 9, pp. 1281-1289.

Card, A., 1982. Using Known Map Categorical Marginal Frequencies to Improve Estimates of Thematic Map Accuracy. Photogrammetric Engineering and Remote Sensing, Vol. 48 No.3, pp 431-439.

Chavez, P.S., and A.Y. Kwarteng, 1989. Extracting Spectral Contrast in Landsat Thematic Mapper Image Data Using Selective Principal Component Analysis. Photogrammetric Engineering and Remote Sensing, vol.55, No. 3, pp 339-348.

Chuvieco, E., and R. Congalton, 1988. Using Cluster Analysis to Improve the Selection of Training Statistics in Classifying Remotely Sensed Data, Photogrammetric Engineering and Remote Sensing, Vol. 56, No. 9, pp 1275-1281.

Congalton, R., 1991. A Review of Assessing the Accuracy of Classifications of Remotely Sensed Data. Remote Sensing of Environment, 37:35-46.

Congalton, R.G., and Mead, R.A. 1983. A Quantitative Method to Test for Consistency and Correctness in Photo-Interpretation, Photogrammetric Engineering and Remote Sensing, Vol. 49, No. 1, pp. 69-74.

Crist, E. P., and Cicone, R. C., 1984. A Physically-Based Transformation of Thematic Mapper data - the TM Tasseled Cap. IEE Transactions on Geoscience and Remote Sensing, Vol. GE-22, pp. 256

Curran, P.J., 1985. Principles of Remote Sensing. Longman, New York. 282pp.

DeGloria, S. D., 1984. Spectral Variability of Landsat-4 Thematic Mapper and Multispectral Scanner Data for Selected Crop and Forest Cover types, IEE Transactions on Geoscience and Remote Sensing, Vol. GE-23, No. 3, pp. 303-311.

EASI/PACE, 1992. Using PCI Software, Version 5.1.

Eby, J. R. 1987. The Use of Sun Incidence Angle and Infrared Reflectance Levels in Mapping Od-Growth Coniferous Forests. Proceedings, American Society for Photogrammetry and Remote Sensing, Fall convention. Reno, Neveda. pp. 36-44.

Eder, J. J., 1989. Don't Shoot Unless its Autumn, Journal of Forestry, 87(6):50-51.

Eyre, F. H., 1980. Forest Cover Types of the U.S. and Canada, Society of American Foresters, Washington, D. C., 148pp.

Fiorella, M., and W. J. Ripple., 1993. Determining Successional Stage of Temperate Coniferous Forests with Landsat Satellite Data. Photogrammetric Engineering and Remote Sensing. Vol. 59, No.2, pp 239-246.

Fung, T., and E. LeDrew., 1988. The Determination of Optimal Threshold Levels for Change Detection Using Various Accuracy Indices. Photogrammetric Engineering and Remote Sensing,Vol. 54, No. 10, pp. 1449-1454.

Green, K., and J. Teply, 1991. Old Growth Forest: How Much Remains, Geo Info Sytems, 1(4): 22-31.

Harris, L.D., 1984. The fragmented Forest. Island Biogeography Theory and Preservation of Biotic Diversity. University of Chicago Press, Chicago. 221pp.

Hopkins, P. F., A. L. Maclean, and T. M. Lillesand., 1988. Assessment of Thematic Mapper Imagery for Forestry Applications Under Lake States Conditions. Photogrammetric Engineering and Remote Sensing, vol. 54, No. 1, pp 61-68.

Hord, R.M., and W. Brooner, 1976. Land-Use Map Accuracy Criteria. Photogrammetric Engineering and Remote Sensing, vol.,42, No. 5, pp 671-677.

Horler, D. N., and F. J. Ahern, 1986. Forestry Information Content of Thematic Mapper Data. International Journal of Remote Sensing, 1(3):405-428.

Ingram, K. J., E. Knapp, and J. W. Robinson, 1981. Change Detection Technique Development for Improved Urbanized Area. Photogrammetric Engineering and Remote Sensing, vol. 49, No. 9, pp 1303-1314.

Jensen, J.R., 1986. Introductory Digital Image Processing: A Remote Sensing Perspective. Prentice-Hal, Englewood Cliffs, N.J. 379pp.

Jensen, J.R. (editor), 1983. Urban/Suburban Land Use Analysis. Manual of Remote Sensing, Vol.2, Second edition (Falls Church, Virginia:American Society of Photogrammetry). pp 1571-1666.

Kalensky, Z., and R.R. Scherk, 1975. Accuracy of Forest Mapping from Landsat Computer Compatible Tapes, Proceedings of the 10th International Symposium on Remote Sensing of Environment, 6-10 October (Ann Arbor, Michigan), pp. 1159-1167.

Latty, R. S., and R. M. Hoffer, 1981. Computer-Based Classification Accuracy Due to the Spatial Resolution Using Per-Point Versus Per-Field Classification Techniques, Proceedings, Symposium on Machine Processing of Remotely Sensed Data, LARS, Purdue University, Indiana, pp. 270-279.

Leprieur, C. E., J. M. Durand, and J. L. Peyron, 1988. Influence of Topography on Forest Reflectance Using Landsat Thematic Mapper and Digital Terrain Data. Photogrammetric Engineering and Remote Sensing, 54(4):491-496.

Lillesand, T.M., and Kiefer, R.W., 1994. Remote Sensing and Image Interpretation, Third edition, Wiley and Sons, New York. 750pp.

Macmillan Bloedel Limited, 1989. Management Plan Carmanah Valley, Folio I. 54pp.

Miller, J. R., J. Wu, M. G. Boyer, M Berlanger, and E. W. Hare, 1991. Seasonal Patterns in Leaf Reflectance characteristics, International Journal of Remote Sensing, 12(7): 1509-1523.

Moffet, M. W., 1997. Tree Giants of North America. National Geographic Magazine, Vol. 191, No. 1, pp. 44-61

Peterson, D. L., W. E. Westman, N. J. Stephenson, V. G. Ambrosia, J. A. Brass and M. A. Spanner, 1986. Analysis of Forest Structure Using Thematic Mapper Simulator Data, IEE Transactions on Geoscience and Remote Sensing, Vol. GE-24, No. 1, pp. 113-120.

Ripple, W. J., S. Wang, D. L. Isaacson, and D. P. Paine, 1991. A Preliminary Comparison of Landsat TM and Spot-1 HRV Multispectral Data for Estimating Coniferous Forest Volume, International Journal of Remote Sensing, 12(9): 1971-1977

SAS Institute Inc., 1988. SAS Language Guide for Personal Computers, Release 6.03 Edition. Cary, NC: 558p.

Singh, A., 1989. Digital Change Detection Techniques Using Remotely Sensed Data, International Journal of Remote Sensing, Vol. 10, No. 6, 989-1003.

Singh, A., and Harrison, 1985. Standaredized Principal Components, , International Journal of Remote Sensing, 6, 883-896.

Schowengerdt, R. A., 1983. Techniques for Image Processing and Classification in Remote Sensing, Academic Press, New York, 249 p.

Shepherd, J.R., 1964. A Concept of Change Detection. Photogrammetric Engineering and Remote Sensing. No. 30, 648-651.

Spies, T.A., J.F. Franklin, and M. Klopsch, 1990. Canopy Gaps in Douglas-Fir Forests in the Casaced Mountains. Canadian Journal of Forest Research. 20:649-658.

Spanner, M.A., J. A. Brass, and D. L. Peterson., 1984. Feature Selection and the Information Content of Thematic Mapper Simulator Data for Forest Structural Assessment. IEE Transactions on Geoscience and Remote Sensing, Vol. GE-22, No. 6, pp 482-489.

Spanner, M. A., L. L. Pierce, D. L. Peterson, and S. W. Running, 1990. Remote Sensing of Temperate Coniferous Forest Leaf Area Index. The Influence of Canopy Closure, Understory Vegetation, and Background Reflectance. International Journal of remote Sensing. 11(1):95-111.

Townshend, J. R. G., 1984. Agricultural Land-Cover Discrimination Using Thematic Mapper Spectral Bands. International Journal of Remote Sensing, Vol. 5, No. 4, pp 681-698.

Townshend, J.R.G., J.R. Gayler, J.R. Hardy, M.J. Jackson and J.R. Baker, 1983. Preliminary Analysis of Landsat-4 Thematic Mapper. International Journal of Remote Sensing, 4, 817.

Tucker, C.J., J.R.G. Townshend, and T.E. Goff, 1985. African Land-Cover Classification Using Satellite Data, Science, 228(4685): 369-375.

Vogelmann, J. E. and B. N. Rock, 1989. Use of Thematic Mapper Data for the Detection of Forest Damage Caused by the Pear Thrips, Remote Sensing of Environment, 30:217-225.

Walsh, S. J., 1980. Coniferous Tree Species Mapping Using Landsat Data, Remote Sensing of Environment, 9:11-26.

Williams, R. S., Jr., 1983. Chapter 31, Geological Application, Manual of Remote Sensing, American Society of Photogrammetry, Vol. 2, pp. 1667-2100.

Wolter, P.T., D.J. Mladenoff, G.E. Host and T.R. Crow, 1995. Improved Forest classification in the Northern Lake States Using Multitemporal Landsat Imagery. Photogrammetric Engineering and Remote Sensing. vol. 61, No. 9, pp. 1129-1143.

Appendix I GCPs And Polynomial Transformations

Ground Control Points (GCP's) for June '92 TM data ordered from worst to best residuals.

GCP No.	Set 2 GCP's (UTM 10 U E000)	Set 1 GCP's (PIXEL)	Residual (PIXEL)	Distance
1	(373200.0, 5395100.0)	(151.5, 81.5)	(.42, -.54)	.69
2	(374300.0, 5386200.0)	(256.5, 362.5)	(-.40, -.53)	.66
3	(375100.0, 5396200.0)	(203.5, 30.5)	(-.22, -.44)	.49
4	(376500.0, 5392400.0)	(278.5, 143.5)	(-.45, .14)	.47
5	(379200.0, 5395800.0)	(339.5, 10.5)	(.27, -.37)	.46
6	(372000.0, 5396680.0)	(99.5, 40.5)	(-.39, .22)	.44
7	(372300.0, 5392800.0)	(140.5, 164.5)	(.28, .34)	.44
8	(378500.0, 5390800.0)	(356.5, 179.5)	(.34, .21)	.40
9	(380000.0, 5380400.0)	(486.5, 505.5)	(-.24, -.29)	.38
10	(377830.0, 5381850.0)	(405.5, 476.5)	(.26, .26)	.37
11	(370800.0, 5396300.0)	(64.5, 62.5)	(.30, .19)	.36
12	(373900.0, 5396300.0)	(164.5, 37.5)	(.31, .15)	.34
13	(377100.0, 5395200.0)	(276.5, 47.5)	(.31, .14)	.34
14	(377900.0, 5382650.0)	(401.5, 449.5)	(.32, -.10)	.34
15	(376200.0, 5394100.0)	(255.5, 90.5)	(-.33, .07)	.33
16	(375400.0, 5391000.0)	(254.5, 197.5)	(.01, -.32)	.32
17	(368300.0, 5393400.0)	(6.5, 176.5)	(-.09, -.31)	.32
18	(381190.0, 5387550.0)	(468.5, 263.5)	(-.14, .28)	.32
19	(372500.0, 5397600.0)	(108.5, 6.5)	(-.24, .19)	.31
20	(380000.0, 5392300.0)	(392.5, 118.5)	(-.21, .21)	.29
21	(369380.0, 5398560.0)	(.5, .5)	(-.09, .27)	.29
22	(382020.0, 5392500.0)	(456.5, 95.5)	(.24, .15)	.28
23	(369200.0, 5385700.0)	(96.5, 420.5)	(.14, .24)	.28
24	(373500.0, 5383720.0)	(250.5, 450.5)	(-.15, .22)	.27
25	(368700.0, 5395300.0)	(4.5, 111.5)	(.05, -.27)	.27
26	(375400.0, 5388100.0)	(277.5, 292.5)	(.09, .23)	.25
27	(383200.0, 5394100.0)	(481.5, 33.5)	(-.12, -.18)	.21
28	(379850.0, 5388400.0)	(418.5, 246.5)	(-.20, .03)	.20
29	(371800.0, 5388700.0)	(156.5, 301.5)	(.03, -.19)	.20
30	(373600.0, 5390500.0)	(200.5, 228.5)	(.16, -.10)	.19
31	(377800.0, 5396100.0)	(291.5, 12.5)	(-.17, .08)	.19
32	(381950.0, 5385750.0)	(507.5, 315.5)	(.13, -.09)	.16
33	(368430.0, 5390000.0)	(37.5, 286.5)	(-.12, .08)	.15
34	(373900.0, 5388650.0)	(224.5, 286.5)	(-.13, .06)	.15
35	(369400.0, 5397900.0)	(6.5, 21.5)	(.05, -.03)	.06
36	(381500.0, 5394900.0)	(420.5, 21.5)	(-.02, .00)	.02
			RMS=(.28, .29)	.40

Polynomial Transformation

Results of least-square regression analysis for the two co-ordinate transformation were as follows:

$x = 0.440+E05 - 0.234X + 0.0013Y - 0.857E-08XY + 0.774-06X^2 - 0.109E-08Y^2$
$- 0.195E-13X^2Y - 0.209E-14XY^2 - 0.593E-12X^3 - 0.374E-30Y^3$

$y = 0.272E+06 - 0.747X - 0.129Y + 0.355E-07XY - 0.227E-05X^2 + 0.152E-07Y^2$
$+ 0.480E-12X^2Y - 0.367E-13XY^2 - 0.290E-12X^3 - 0.142E-28Y^3$

where x, y are distorted image co-ordinates (pixel/column; line/row) and X, Y are UTM (map) co-ordinates.

Residual Plot (PIXEL):

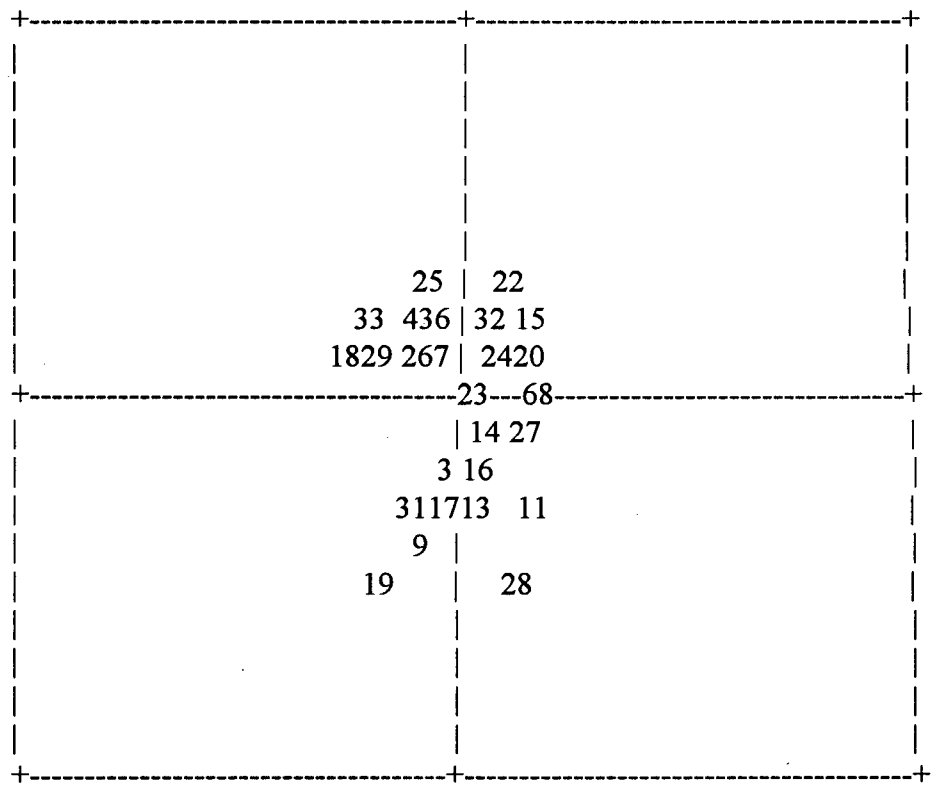

Appendix II Signature Separability Reports

Divergence matrix for forest training classes in June TM data

	ncc	occ	reg	juv	scru	ch	sh	nc	dch	alp	uc	chb
occ	2.00											
reg	2.00	2.00										
juv	2.00	2.00	1.98									
scru	2.00	2.00	2.00	2.00								
ch	2.00	2.00	2.00	2.00	1.77							
sh	2.00	2.00	2.00	1.99	1.99	1.98						
nc	2.00	2.00	2.00	2.00	2.00	1.99	1.99					
dch	2.00	2.00	2.00	2.00	2.00	1.99	1.99	1.25				
alp	2.00	2.00	1.99	1.23	2.00	2.00	1.94	2.00	2.00			
uc	2.00	2.00	2.00	1.96	1.99	1.99	1.99	2.00	2.00	1.88		
chf	2.00	2.00	2.00	2.00	1.98	1.82	1.79	1.99	1.99	2.00	1.99	

Divergence matrix for forest training classes in September TM data

	ncc	occ	reg	juv	scru	ch	sh	nc	dch	alp	uc	chb
occ	2.00											
reg	2.00	2.00										
juv	2.00	2.00	1.99									
scru	2.00	2.00	2.00	2.00								
ch	2.00	2.00	2.00	2.00	1.85							
sh	2.00	2.00	2.00	1.99	1.99	1.96						
nc	2.00	2.00	2.00	2.00	2.00	2.00	2.00					
dch	2.00	2.00	2.00	2.00	1.99	1.93	1.90	2.00				
alp	2.00	2.00	1.99	1.42	2.00	2.00	1.99	2.00	2.00			
uc	2.00	2.00	1.99	1.89	2.00	2.00	1.99	2.00	2.00	1.96		
chf	2.00	2.00	2.00	1.99	1.99	1.94	1.12	2.00	1.34	1.99	1.99	

This method gave real values between 0 and 2 where 0 indicated a complete overlap between signatures and 2 indicated a complete separation between any two classes. A value below 1.5 indicated spectrally similar classes. Classes with at least 1.5 and above were statistically separable and deemed suitable for classification.

Appendix III. PCA and Change Detection Images

Figure 16. Enhanced PC1, PC2 and PC3 colour composites. Black is water, purple is clearcuts, violet is scrubland, orange is shoreline/creeks and, blue, green and green-yellow are forest stands.(a) June, 1992 enhanced composite with cloud cover appearing in yellow over the subscene. (b) September, 1992 enhanced composite.

(a)

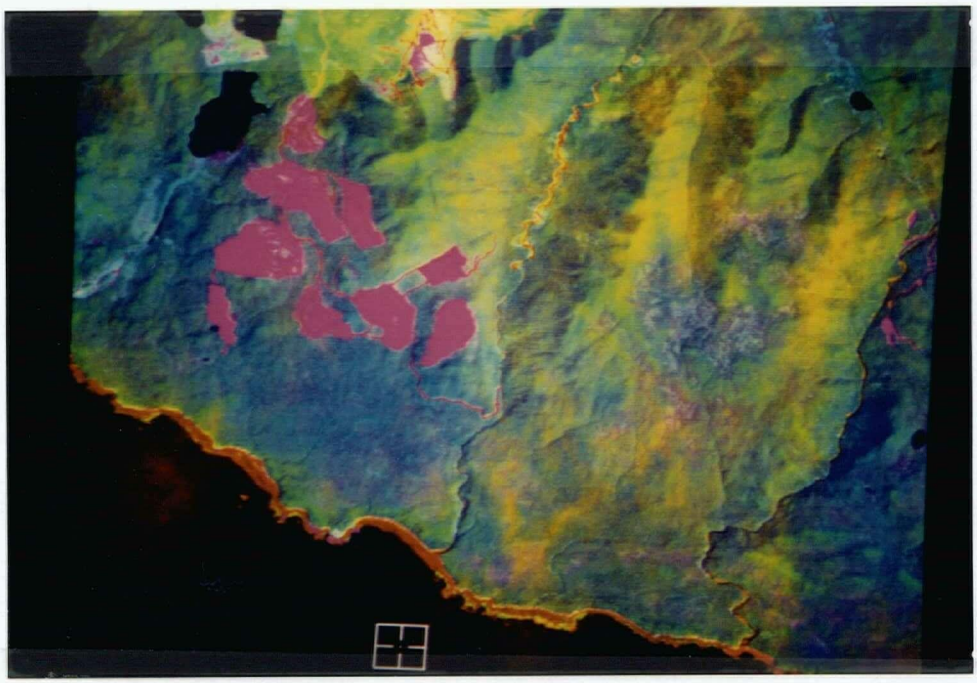

(b)

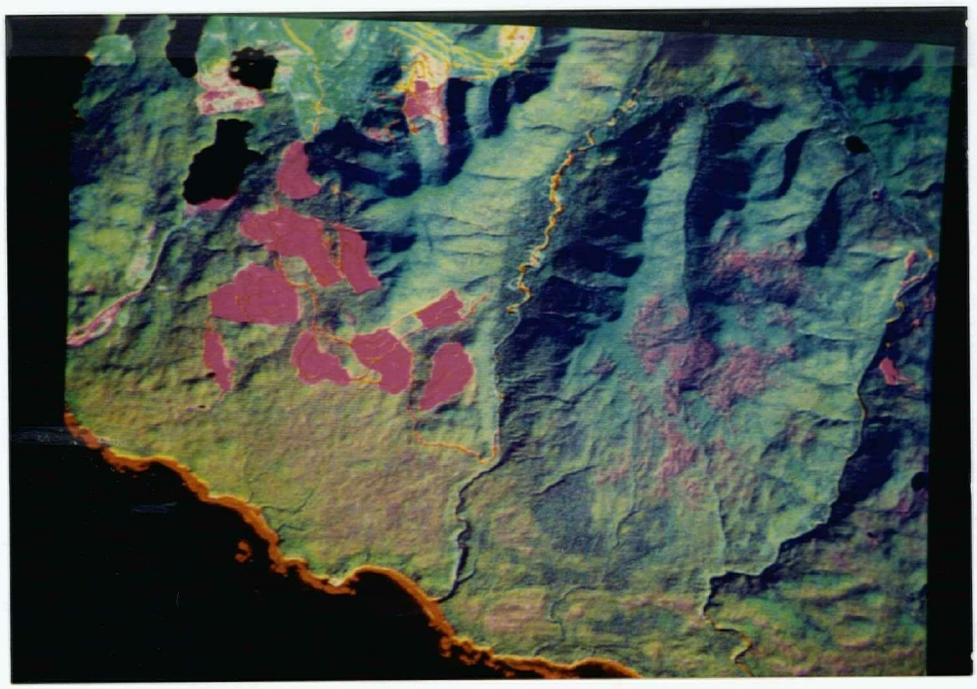

Figure 17. Change detection images generated using image ratioing. Black is clearcuts/logging roads, white (bright tones) is water bodies, gray/moderate tones is forest stands. (a) TM63/TM93 image ratio (b) TM67/TM97 image ratio.

(a)

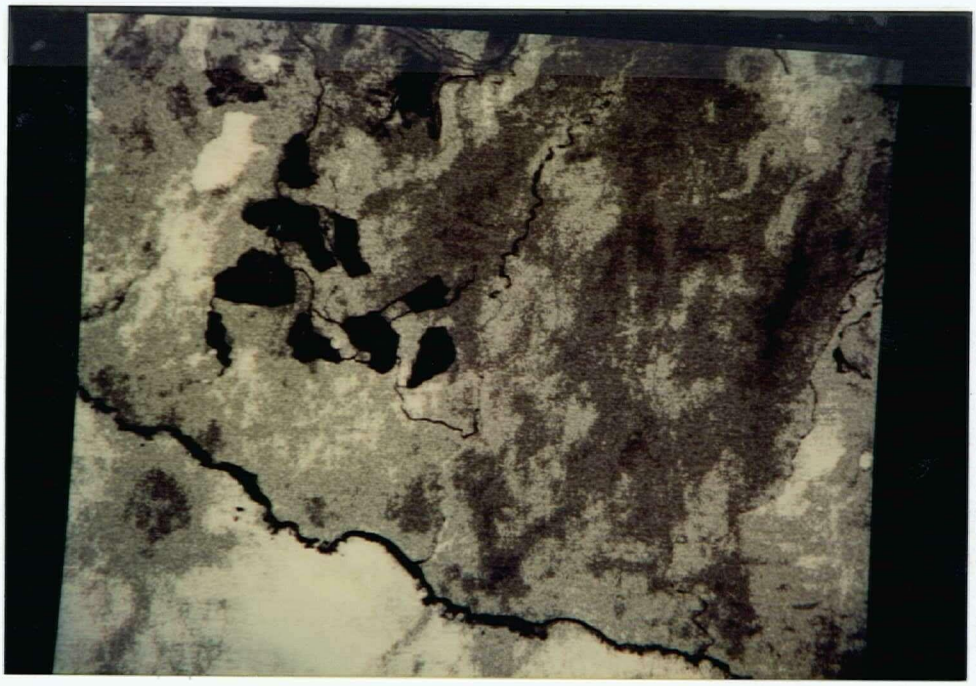

(b)

Appendix IV. Analysis of Variance Procedure for Classification Accuracy

Dependent Variable : General Cover Type Classification Accuracy.

Source	DF	Sum of Squares	Mean Square	F Value	Pr > F
Model	2	1449.2026	724.6013	7.23	0.0021
Error	39	3906.5246	100.1673		
Corrected Total	41	5355.7272			

Dependent Variable : Forest Cover Type Classification Accuracy.

Source	DF	Sum of Squares	Mean Square	F Value	Pr > F
Model	2	1900.2519	650.2519	16.50	0.0001
Error	24	1381.8502	57.5771		
Corrected Total	26	3282.3541			